Experimental Comparison of Skid Steering Vs. Explicit Steering for a Wheeled Mobile Robot

Benjamin Shamah

CMU-RI-TR-99-06

Submitted in partial fulfillment of the
requirements for the degree of
Master of Science
in the field of Robotics

The Robotics Institute
Carnegie Mellon University
Pittsburgh Pennsylvania 15213
March 1999

Abstract

Robotic tasks call for a range of steering activity: one extreme is highway driving with negligible turning for hundreds of kilometers; another is forklift handling, which calls for agile turning. The scope of this thesis considers steady state turning of a wheeled vehicle on natural terrain with slow but capable locomotors characteristic of planetary robotic vehicles.

Experiments are performed using a single vehicle that can exhibit both skid and explicit steering while driving steady state circles. Skid steering is accomplished by creating a differential velocity between the inner and outer wheels. Explicit steering is accomplished by changing the heading of the wheels to cause a change in heading of the vehicle. Experimental results are gathered to provide information regarding power draw, individual wheel torque, and position information.

The experimental results show that power and torque for skid and explicit turning degenerate to equal values at infinite radius (straight driving). As the turn radius decreases from straight driving to a point turn, greater power and torque are required as a greater sideslip angle is encountered. For all turns skid steering requires greater power and torque than for explicit turning because sideslip angles are greater in all cases. In the limiting case of a point turn, the power for skid steering is approximately double that of an explicit point turn. The primary contribution of this research is the experimental quantification of the power and torque requirements over turn radii from zero to infinity.

Table of Contents

Table of Contents

List of Tables

List of Tables

List of Figures

List of Figures

Acknowledgements

First, I would like to thank my family and friends for all of their support over the years which has helped me to overcome the various challenges along the way.

Red Whittaker has not only served as my advisor but as a constant inspiration to accomplish the impossible. He has taught me not only how to examine a problem but how to execute the solution under any circumstances.

This thesis would not have been possible without the construction of the robot Nomad. I would like to thank Eric Rollins, Mark Sibenac, Mike Parris, and Jim Teza for all of their efforts in the construction and deployment of Nomad. The development of Nomad is an experience that I will never forget.

My sincere appreciation goes out to all of my committee members: Red Whittaker, John Bares, Matt Mason, and Dimi Apostolopoulos. Dimi has been a significant inspiration for me in the field of robotic locomotion. Without Dimi's calming advice I know that I would not have accomplished as much as I have over the last two years.

I would like to thank Stewart Moorehead and Matt Deans for their help in discussing tactics for data analysis.

Dot Marsh has gone out of her way on countless occasions to make sure that everything was in place for me to reach my goals.

Chapter 1 Introduction

1.1 Robotic Steering

Robotic tasks call for a range of steering activity: one extreme is highway driving with negligible turning for hundreds of kilometers, another is forklift handling which calls for agile turning. This thesis investigates the roles of propulsion and steering for a range of steering activity.

Skid steering can be compact, light, require few parts, and exhibit agility from point turning to line driving using only the motions, components, and swept volume needed for straight driving. The downside is that skidding causes unpredictable power requirements. Skid steering also fails to achieve the most aggressive steering possible which can be achieved with explicit steering. Skid steering while traveling up a slope will be inhibited before explicit steering is inhibited. Explicit steering points the wheels in the direction of travel so that skidding is minimized. The advantage of explicit steering is more aggressive steering with better dead reckoning and lower power consumption. The downside of explicit steering is a higher actuator count, part count, and the necessary volume sweep.

Another significant difference between skid and explicit steering is the transmission of torque. For skid steering the motion of the wheels is limited to rotation about one axis. Therefore, a centralized drive can pass the drive torques directly to each wheel. For explicit steering since the wheels move about two axes the torque transmission is more difficult. If a centralized drive is used the torque must pass through universal joints and drive shafts which have inefficiencies. Another approach for explicit steering is to use individual drive motors inside of each wheel with the necessary gearing. Although the transmission of drive torque for explicit steering is complex, the lateral forces observed in skid steering are significantly higher than those in explicit steering. Therefore, the structure supporting the wheels must be stronger than that used for explicit steering.

The merits of steering depend on the task and the terrain. For example, steering efficiency

and aggression are unimportant for driving on a straight, flat road. Alternately, torturous agility might require excessive turning. Examples include reversals and three point turns.

This thesis seeks to answer the question: what are the merits of skid steering and explicit steering in the context of varying steering activities? The scope of this thesis considers steering on natural terrain with slow but capable locomotors of the type applicable to planetary driving.

This thesis does not consider high speed driving or road vehicles such as passenger cars. Off road equipment such as bulldozers and loaders (which exhibit high locomotion and maneuverability at the expense of mass and power) are not covered. This thesis considers the simple classification of skid and explicit steering. Within these classes only the experimental results exhibited by the Nomad robot are used. Although Nomad steers its four wheels by driving four bar linkages, the resulting wheel motion is analogous to that achieved by chassis articulation or four wheel Ackerman steering.

Nomad

size stowed: 1.8m x 1.8m x 2.4m

size deployed: 2.4m x 2.4m x 2.4m

mass: 725 kg

total power

consumption: 3500 W max

Figure 1: Nomad

1.2 Objective

The objective of this thesis is to analyze the behavior of skid steering and explicit steering in terms of power draw, torque, and slip. Experimental results will be presented in an attempt to detail the advantages and disadvantages of each mode with respect to a wheeled robotic explorer traversing off-road terrain.

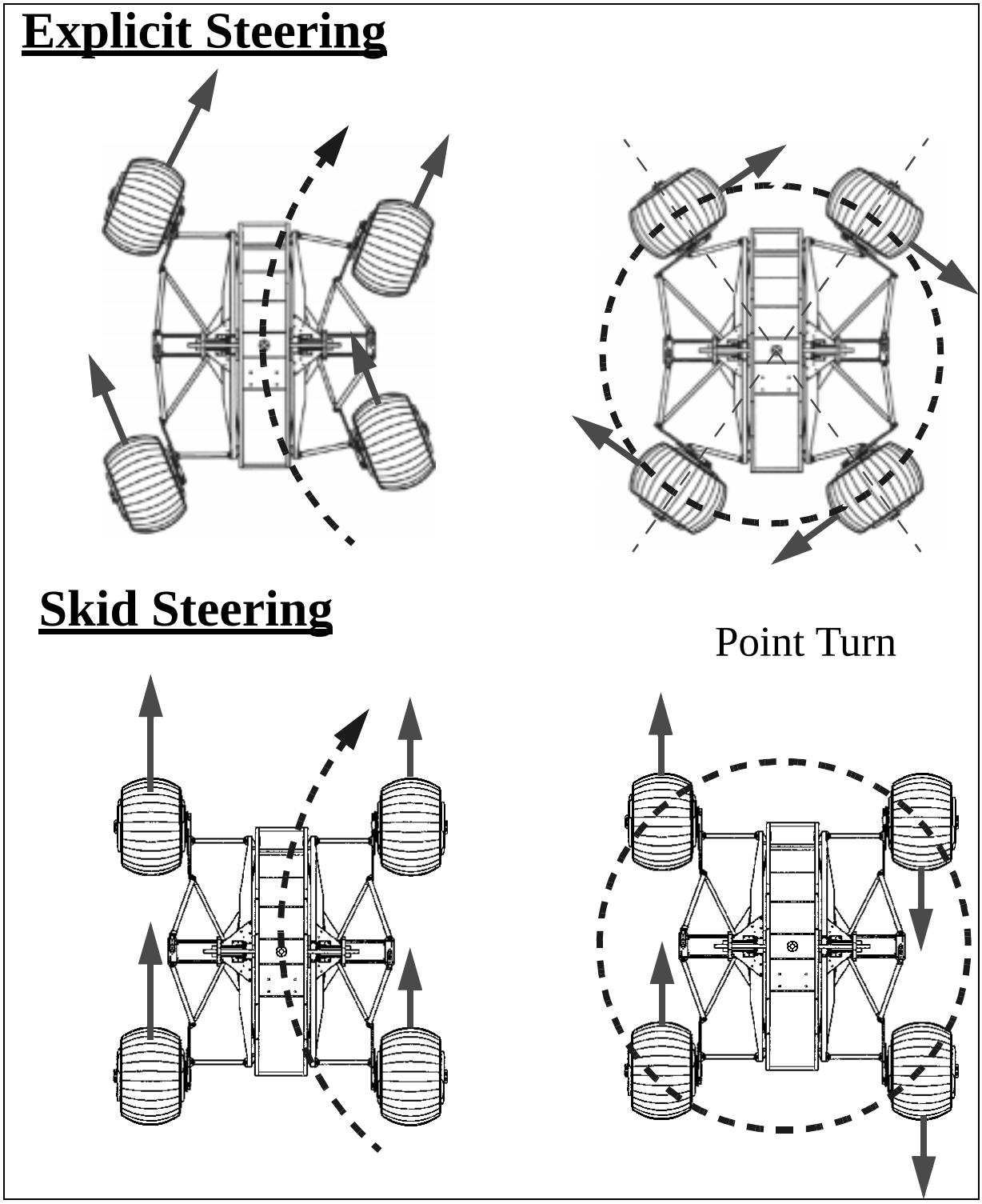

Figure 2: Nomad Steering Modes

1.3 Problem Statement

Quantification of the amount of power used for both explicit and skid steering is needed to allow educated decisions to be made about which steering configuration is appropriate for a specific application. Mission planning is used to determine the actions of a robot to perform a goal. The plan can be optimized over many criteria, such as energy consumption. For extreme tasks such as planetary exploration and work in hazardous environments, a complete understanding of the energy consumed for different maneuvering can impact the amount of work accomplished by the robot. Depending on the configuration of the robot, a longer path with a large turn radius may be more efficient than a point turn. The empirical study of real systems allows increased understanding of different steering configurations.

1.4 Thesis Statement

This thesis asserts that an empirical study of steady state turning for both explicit and skid steering configurations allows improved decisions to be made about the use of steering configurations on mobile robots.

1.5 Background

The study of steering system forces as defined by the society of automotive engineers provides an introduction to the terminology and the forces acting on a vehicle during a turn. Although a standard automotive chassis is designed for much higher speeds than any planetary exploring vehicle, many of the forces are identical.

For a wheeled vehicle the forces and moments imposed on the steering elements stem from those generated at the tire-ground interface. The coordinate system is based at the bottom of the wheel where the X coordinate is in the direction of wheel travel. The Y coordinate is parallel to the axis of the wheel's rotation and the Z coordinate is perpendicular to the ground. The wheel torque is generated around the axis of rotation and is resisted by the rolling resistance moment. The aligning torque resists any change in the heading of the wheel around the Z axis. The overturning moment resists any lateral forces generated as the wheel slides in the Y direction during a turn. The slip angle α is defined as the difference between the direction in which the wheel is heading and the direction of wheel travel.

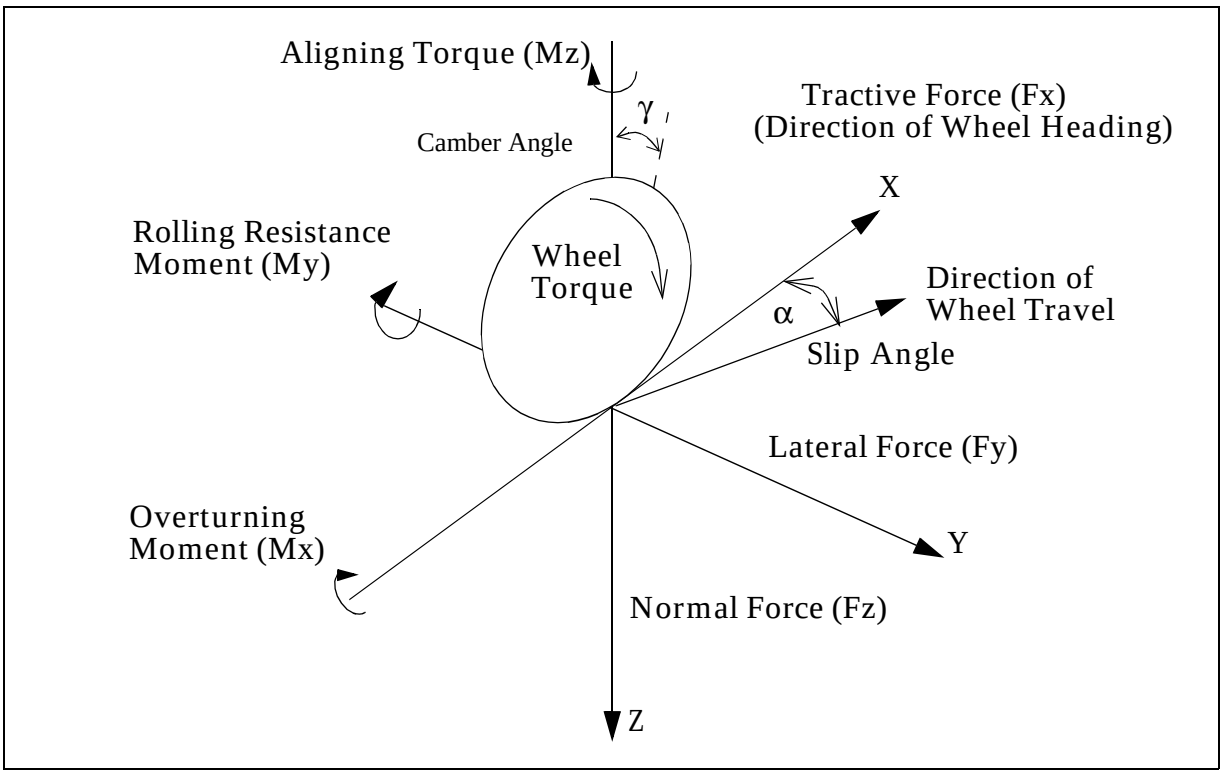

Figure 3: Wheel Axis and Forces [Wong93]

When a driving torque is applied to a wheel the distance that the tire travels is less than that travelled by a tire moving in an unloaded and free rolling condition. This phenomenon is known as longitudinal slip and is described by the following equation [Wong93]:

$$i = \left(1 - \frac{V}{r\omega}\right) \times 100 \qquad [1]$$

Where: i is the longitudinal slip in percent, V is the linear speed of the tire center, r is the rolling radius of the free rolling tire, and ω is the angular speed of the tire. Complete, or 100%, slip occurs when the wheel rotates without any translatory progression. A general theory to accurately define the relationship between the driving torque and the longitudinal slip does not exist.

1.5.1 Steady State Turning

In previous research, a computer simulation of a four wheel drive, four wheel steer tractor showed that the tractor has a tendency to be pulled toward the inside of the turn when the steering angle and the frictional coefficient become large. However, as the running speed increases the tractor has a tendency to be pulled away from the turning center. The

simulation also shows that the turning radius decreases as the tractor's center of gravity is moved toward the rear of the vehicle [Itoh90].

Experiments were performed using a real tractor on a rice field and a paved road. As the steering angle and the running speed were altered, the following parameters were measured: tire forces, slip, and side slip angles. Two free rotating wheels were added to the front and the rear of the vehicle in order to measure slip, assuming that the slip of the rear fifth wheel would be zero.

The lateral forces on the rear tires of the four wheel steer experiments were found to be greater than those occurring when the tractor was operated in a two wheel steer mode. It was then determined that the rear tire steer angles were not theoretically correct and that this problem had caused the increase in lateral resistance.

During tight turns the two wheel steer tractor experienced negative thrust in the front tires. The tight corner braking phenomenon was observed only in the two wheel steer tractor. The simulation did not accurately predict the increase in thrust with an increase in steer angle. Nor did the simulation predict the negative thrust of the two wheel steer tractor [Itoh94].

1.5.2 Steering Configuration

One study of steering configurations, performed in reference to mobile wheeled earthmoving equipment, determined that no one optimum steering system exists for all applications. The optimal system can be determined as a function of operating conditions, special tasks, service life, as well as cost parameters for manufacture. In general small loaders have a wide variety of steering systems; large loaders, on the other hand, are frame articulated. The new trend in optimizing steering systems is in the use of load sensors, which optimize the hydraulic pressure needed to actuate the wheels.

Dudzinski maintains that maneuverability is dependent not only on the steering mechanism but also on steering control. The goal of the steering mechanism is to ensure maneuverability and vehicle stability. Dudzinski evaluates skid steering, single axle steering, double axle steering, and articulated frame steering [Dudzinski89].

The main characteristics of the comparison are based on maneuverability, stability, traction, and design complexity. Power draw is not a critical metric for the earth moving industry as fuel costs are low. Precise vehicle positioning for earthmoving equipment is not as critical because the human operator is capable enough to account for the vehicle's inaccuracies. For a robotic vehicle power draw and positioning become the most critical factors.

1.6 Steering Kinematics

The examination of the kinematics of different steering configurations allows the properties of the different steering modes to be observed in terms of different performance metrics. For example, the occupied volume necessary to allow explicit steering can be viewed by a kinematic analysis. However, any kinematic study is an idealized analysis since the wheel ground interaction is not considered.

1.6.1 Single Axle Steering

For road vehicles, the most common steering configuration is single axle steering in which two wheels are pivoted. In order to minimize lateral forces on the tires during the turn, all wheels should be in a pure rolling condition. The wheels must follow curved paths with different radii originating from a common center. The relation between the steer angle of the inside front wheel and the outside front wheel can be obtained from geometry:

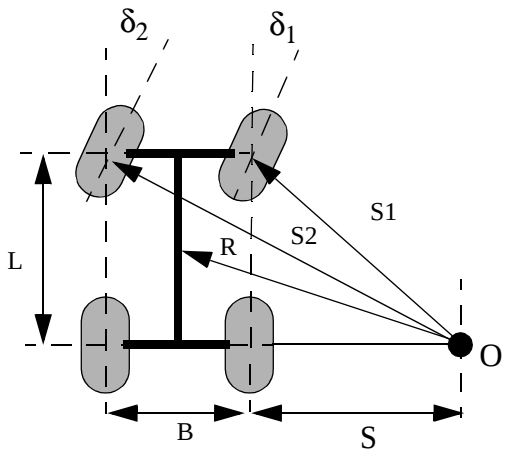

Variables:

δ_2 = outside wheel heading [rad]
δ_1 = inside wheel heading [rad]
R = vehicle radius [m]
L = vehicle length [m]
B = vehicle width [m]
O = turn center location

Figure 4: Single Axle Steering

$$S = \sqrt{R^2 - \left(\frac{L}{2}\right)^2} - \frac{B}{2} \quad [2]$$

$$\delta_1 = tan\left(\frac{L}{S}\right) \quad [3]$$

$$\delta_2 = tan\left(\frac{L}{B+S}\right) \quad [4]$$

Since the outer wheels travel a longer path distance than the inner wheels, the velocity components must be distributed to match the path lengths.

1.6.2 Double axle steering

Four wheel steering offers greater maneuverability than two wheel steering by moving the turn center closer to the vehicle center. A four wheel steer vehicle accomplishes half the turn radius of a two wheel steer vehicle for the same change in wheel heading.

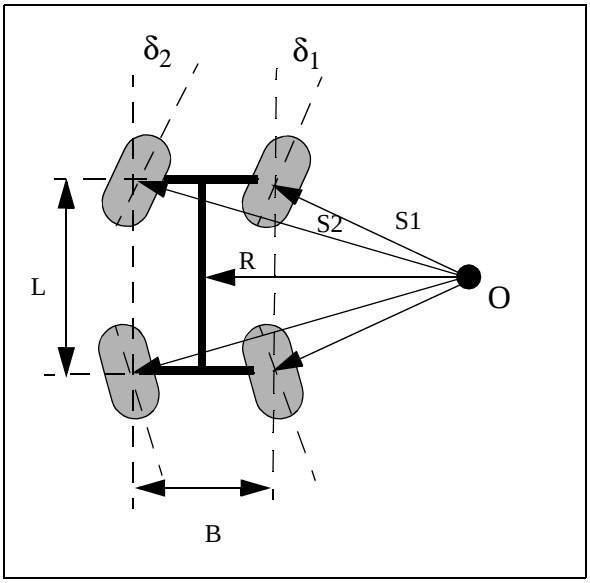

Figure 5: Double Axle Steering

$$\delta_1 = tan\left(\frac{\frac{L}{2}}{R-\frac{B}{2}}\right) \quad [5]$$

$$\delta_2 = tan\left(\frac{\frac{L}{2}}{R+\frac{B}{2}}\right) \quad [6]$$

1.6.3 Skid steering

The kinematic analysis of skid steering allows a preliminary determination of wheel velocities given the vehicle dimensions, the desired radius, and the desired turn rate. However, as in the previous kinematic models, no forces are studied. Therefore, the slippage (which is more prevalent in skid steering) is not accounted for; thus the kinematic model is even less accurate.

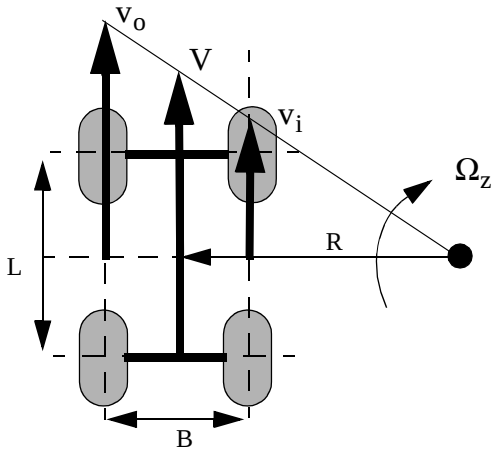

Variables:

v_o = outside wheel velocity [m / s]
v_i = inside wheel velocity [m / s]
V = vehicle velocity [m / s]
Ω_z = vehicle angular velocity [rad / s]
R = vehicle turn radius [m]
L = vehicle length [m]
B = vehicle width [m]

Input Parameters for Nomad

Desired Radius R= 4m, 8m, 12m
Vehicle Velocity: V=0.15 m / s
Vehicle Width: B=1.97 m

Figure 6: Kinematic Skid Steer Model

The radius of the turn can be calculated from similar triangles [Wong93].

$$\frac{v_o}{v_i} = \frac{R + \frac{B}{2}}{R - \frac{B}{2}} \quad [7]$$

$$R = \frac{\frac{B}{2}\left(\frac{v_o}{v_i} + 1\right)}{\left(\frac{v_o}{v_i} - 1\right)} = \frac{B}{2}\left(\frac{v_o + v_i}{v_o - v_i}\right) \quad [8]$$

However, this radius will only be achieved if no slippage occurs between the wheel and the soil. In order to account for the slippage of the outer wheels, i_o and the inner wheels, i_i:

$$R' = \frac{B}{2}\left(\frac{v_o(1 - i_o) + v_i(1 - i_i)}{v_o(1 - i_o) - v_i(1 - i_i)}\right) \quad [9]$$

The turn rate or yaw velocity can be found from the following:

$$\Omega_z = \frac{v_o + v_i}{2R} = \frac{v_i\left(\frac{v_o}{v_i} - 1\right)}{B} \quad [10]$$

Again, in order to account for the slippage:

$$\Omega_z' = \frac{v_o(1 - i_o) + v_i(1 - i_i)}{2R'} = \frac{v_i\left(\frac{v_o(1 - i_o)}{v_i} - (1 - i_i)\right)}{B} \quad [11]$$

Given an accurate slippage model, the kinematic model can be used to provide accurate results. Without a longitudinal slip model, wheel velocities and turn radius can only be assumed to be estimates.

1.7 Steering Activity

The notion of steering activity is the comparison of different driving maneuvers such as highway driving and forklift maneuvering. By quantifying the amount of steering in a path, relative to path and vehicle dimensions, understanding can be gained of the optimal driving mode to be used to traverse a given path. One expression of steering activity is to integrate the total distance traveled by the outer and inner wheels and divide by the total path length of the vehicle center. The shortcoming of this formulation is the singularity that occurs when the outer and inner wheels are moving but the vehicle center does not. Mathematical speculation of the steering activity metric are expressed in Appendix D.

An example of a traverse including several different levels of steering activity is shown in Figure 7. The path of the sojourner rover [Hayati96] shows how during one mission several different modes of driving are used. With the use of a steering activity metric combined with a power or torque model of the type developed in this research it is possible to predict the energy and peak power needed by a robot to complete a given traverse. This enables a more rigorous understanding of robot design and performance which can be applied to the optimization of mission planning.

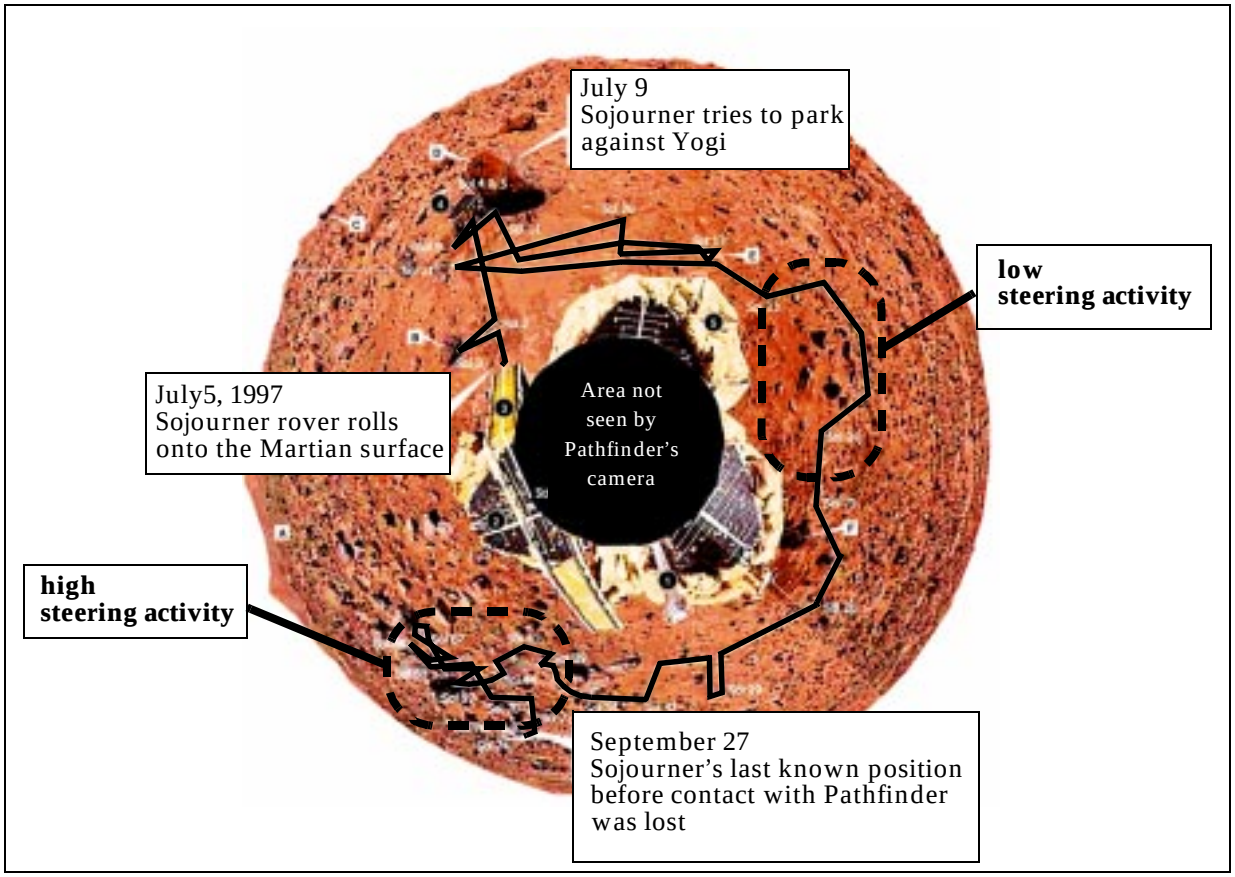

Figure 7: Traverse of Sojourner on Mars [nytimes98]

Chapter 2 Methodology

2.1 Approach

In order to compare explicit and skid steering in this investigation, empirical performance is derived from experimental data. The data is gathered using a vehicle that can change its wheel heading for explicit steering and lock the wheel heading for skid steering. Steady state turning is evaluated using gps as a measure of independent absolute position, which can be post processed to determine the radius of each turn. Using measurements of wheel velocity as well as current and voltage values, torque and power are computed for each in wheel drive unit.

2.2 Experimentation

The experiments consider steady state turning which does not include the transition from driving straight into a turning condition. All experiments are performed on flat terrain in an outdoor environment. The terrain is naturally flat and without obstacles. However, locally varying slopes up to +/- 2 degrees and terrain inconsistencies are encountered.

2.3 Description of Experiments

The experiments cover explicit and skid turning over a range of turning radii. For each case an infinite radius (equivalent to straight driving), 12 m, 8m, 4m, and a 0m or point turning is studied at a vehicle velocity of 15 cm/s. For each test 22 data signals are recorded as shown in Table 2. The PID controller used on the velocity loop for the drive motors does not change during any of the experiments (as described in Appendix C). The nominal direction of turn studied is clockwise. However, the 4m radius turn is studied in both the clockwise and couterclockwise direction to examine inconsistencies.

2.3.1 Infinite Radius

An infinite radius, or straight driving, is commanded for a single test at 15 cm/s. Only one test is necessary because explicit and skid steering are equivalent at an infinite radius. The duration of the test is one minute of driving. All wheels are commanded a velocity of 15 cm/s without any type of feedback loop to control the direction of travel of the vehicle.

2.3.2 Radius: 4, 8, and 12 m

The kinematics of Nomad's explicit steering are used to provide the correct wheel angles for each explicit turn. Data is recorded while Nomad is in a steady state turn so that no information regarding the transition into the turn is recorded.

The kinematic skid steer model is used to compute wheel velocities as described in Chapter 1. Due to the inaccuracies of the kinematic model the wheel velocities are modified experimentally until Nomad traverses the desired radius while holding a vehicle velocity of 15 cm/s.

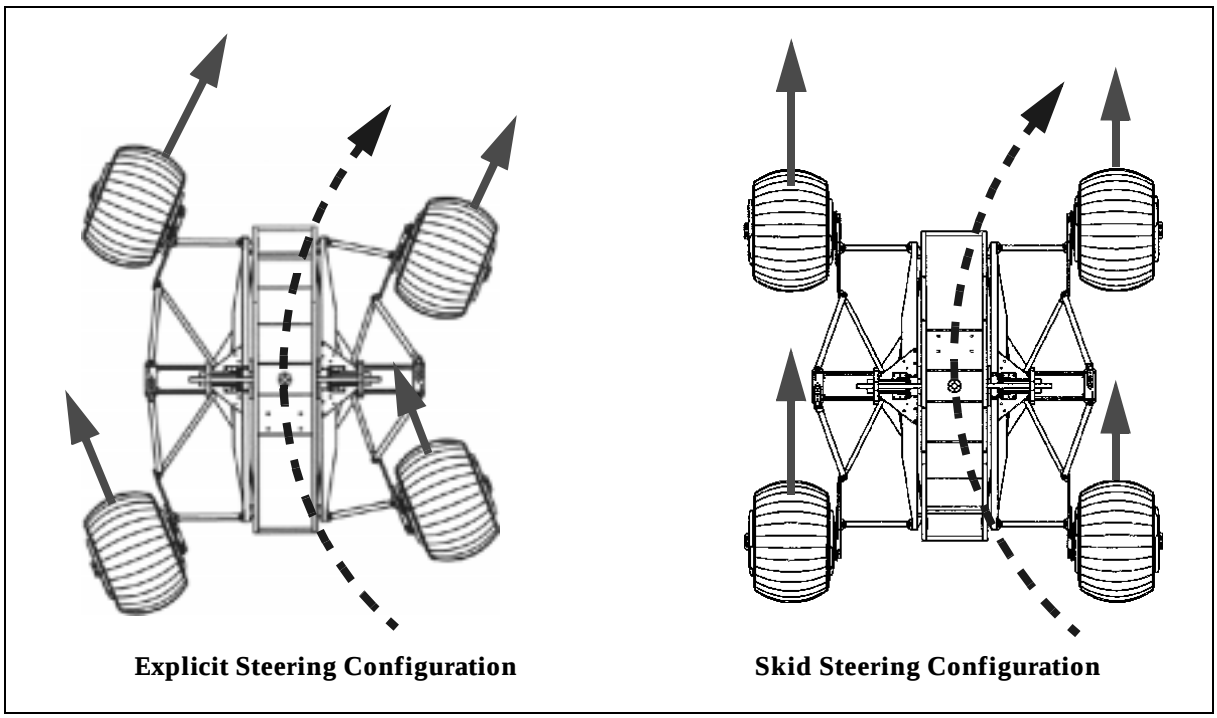

Figure 8: Explicit and Skid Turning Configurations

From similar triangles the theoretical values for the ratio of outer and inner wheel velocities are calculated as described in Chapter 1. Using the vehicle velocity of 15 cm/s the outer and inner wheel velocities v_o and v_i are identified as shown in Table 1.

Table 1: Theoretical Skid Steering Velocity Values

Desired Radius [m]	*V [m/s]*	v_i *[m/s]*	v_o *[m/s]*
4	**0.15**	**0.11**	**0.19**
8	**0.15**	**0.13**	**0.17**
12	**0.15**	**0.14**	**0.16**

2.3.3 Point Turn

Point turning is the limiting case of tight turning as the radius approaches zero. For the explicit point turn the configuration of the wheels is such that the axis of rotation of diagonal wheels are aligned (the right front and the left rear, the left front and the right rear) as shown in Figure 9. All wheels are commanded a velocity of 15 cm / s.

For a skid steer point turn the outer and inner wheels are given equal and opposite wheel velocities of 15 cm / s. The skid steer point turn shows the most dramatic side slip angle in which the direction of thrust provided by the wheels is almost perpendicular to the actual direction of motion of the wheel as the vehicle turns.

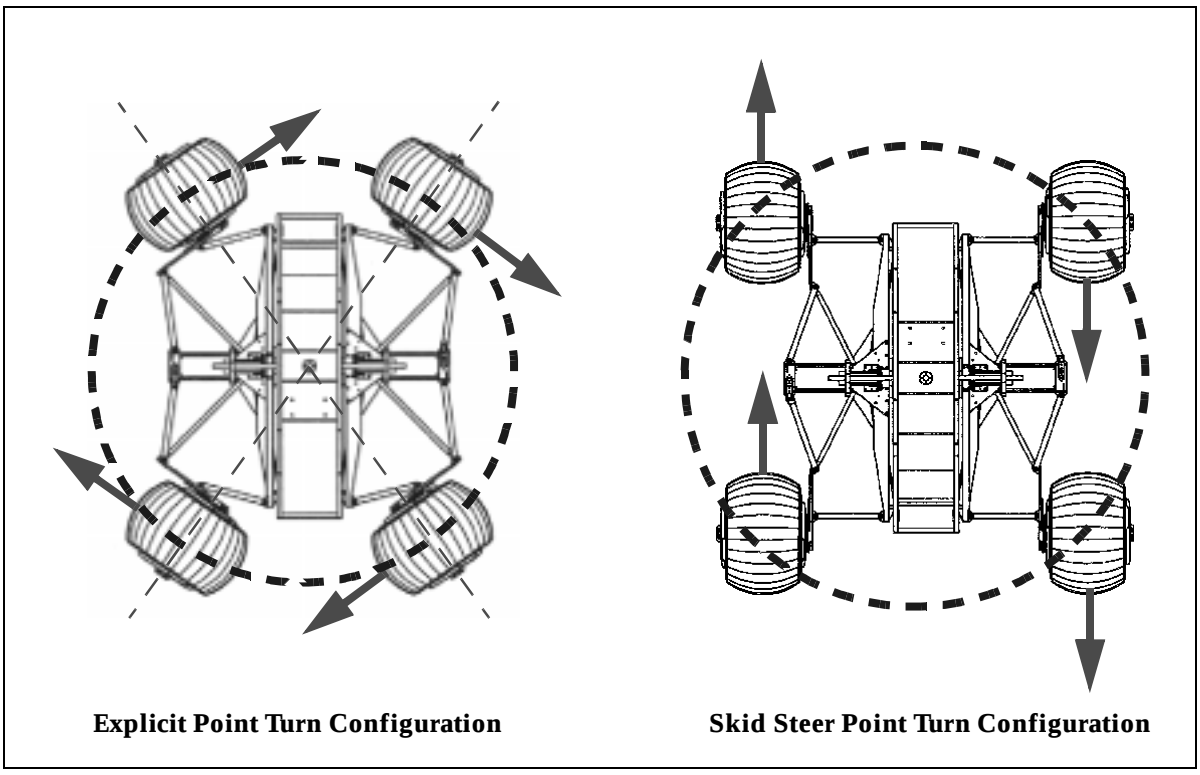

Explicit Point Turn Configuration **Skid Steer Point Turn Configuration**

Figure 9: Explicit and Skid Point Turning Configurations

2.4 Method

During the experiments Nomad is teleoperated from a command station in view of all maneuvers. Velocity commands are given for each wheel as well as a steering command. During the skid steer experiments the steering motors hold the linkages in the position for straight driving. However, the steering motors do not servo to a given position.

Sensor readings from Nomad are recorded using a real-time stethoscope that monitors

Table 2: Sensor Readings from Nomad

Item	*Units*	*Sensor*	*Notation*
Pitch of the Robot	radians	Digital Gyro Compass	ϕ
Roll of the Robot	radians	Digital Gyro Compass	θ
X coordinate of the robot with respect to the base station	meters	Differential GPS	X
Y coordinate of the robot with respect to the base station	meters	Differential GPS	Y
Steering Linkage Position - Left	radians	encoder	RollerDist_L
Steering Linkage Position - Right	radians	encoder	RollerDist_R
Drive Actuators (x 4)			
Motor shaft position	radians	encoder	drive0_Angle
Commanded current	amps	real time computer	drive0_CurrentCom
Current draw after the amp	amps	current monitor	drive0_CurrentMon
Current draw before the amp	amps	current sensor	drive0_CurrentSens

and records the 22 signals.

The robot position is monitored by the use of a digital gyro compass and differential gps. The compass has an update rate of 20 Hz and an accuracy of +/- 1 degree for both the pitch and roll of the body of Nomad (which is the average of the disturbance taken by the four wheels due to the body averaging). The distance from Nomad to a stationary base station is provided by differential gps. The base station is placed at the same location each time experiments are performed. The X and Y coordinates are the distances from the antenna located on Nomad to the differential base station and are updated at 5 Hz with an accuracy of +/- 10 cm.

Information from the four wheel actuators is recorded at 60 Hz from the real time system.

The linear velocity is calculated using the encoder position, the time stamp, the gear reduction, and the wheel diameter.

The observed current is essentially identical to the commanded current, which monitors whether the servocontrol is operating appropriately. The current sensors are implemented to monitor the power draw of the amplifier for each drive actuator. The drive power is computed by multiplying the voltage by the value of the current sensor.

Chapter 3 Nomad

3.1 Nomad: An Experimental Testbed

In terms of steering evaluation the configuration of Nomad [Bapna97] provides the unique ability of having one platform that can achieve two different steering modes over a complete range of radii. The steering modes being investigated are explicit and skid steering, including point turns. The integration of independent wheel control with the transforming chassis enables the steering modes. The following sections describe the locomotion subsystem details.

3.2 Transforming Chassis

Nomad's transforming chassis enables explicit steering while keeping a low center of gravity and expanding the footprint of the robot into a deployed position, increasing stability. The transforming chassis is based on the motion of four bar linkages connected to each wheel. The wheels are actuated in pairs such that the right wheels move synchronously (as do the left wheels). Each wheel is actuated by a pushrod connected to the axis of rotation of the output link. The pushrod is also attached to a block which slides along a linear rail. The block is attached to a rack which is actuated by the steering motor.

The kinematics of the transforming chassis are needed to minimize resistance and internal forces during explicit steering maneuvers. The goal of the kinematic analysis is to produce the necessary geometric positions of the linkage sets such that the inner and outer wheels roll on concentric arcs.

Turning commands are transformed into actuator inputs that control the motion of point F and control individual wheel velocities. The turning radius is calculated as a function of the actuator input, computing the appropriate wheel velocities and using lookup tables to reverse the calculations. The transformation is done separately for each side of the vehicle so that the vehicle turns on a radius given for the center of the vehicle while each set of wheels rolls on concentric arcs.

The lookup table is created by varying the position of point F along its constrained path and calculating both the steering angle δ and the wheel position E. Then the radius for that wheel is calculated as a function of δ and E as shown in Figure 10 [Rollins98].

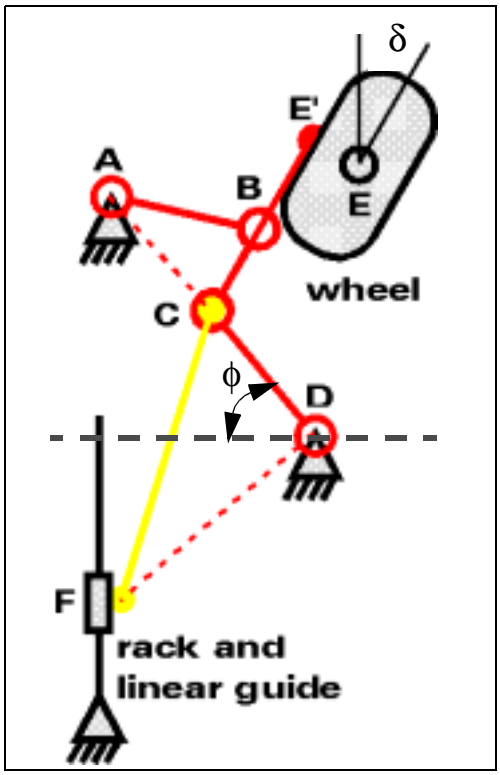

Figure 10: Transforming Chassis Diagram

Figure 11 shows the incremental steps completed as Nomad deploys the right side of the chassis from the stowed position to the explicit point turn position. Notice that steps three and five are not only part of the deployment phase but are also steering positions for the chassis.

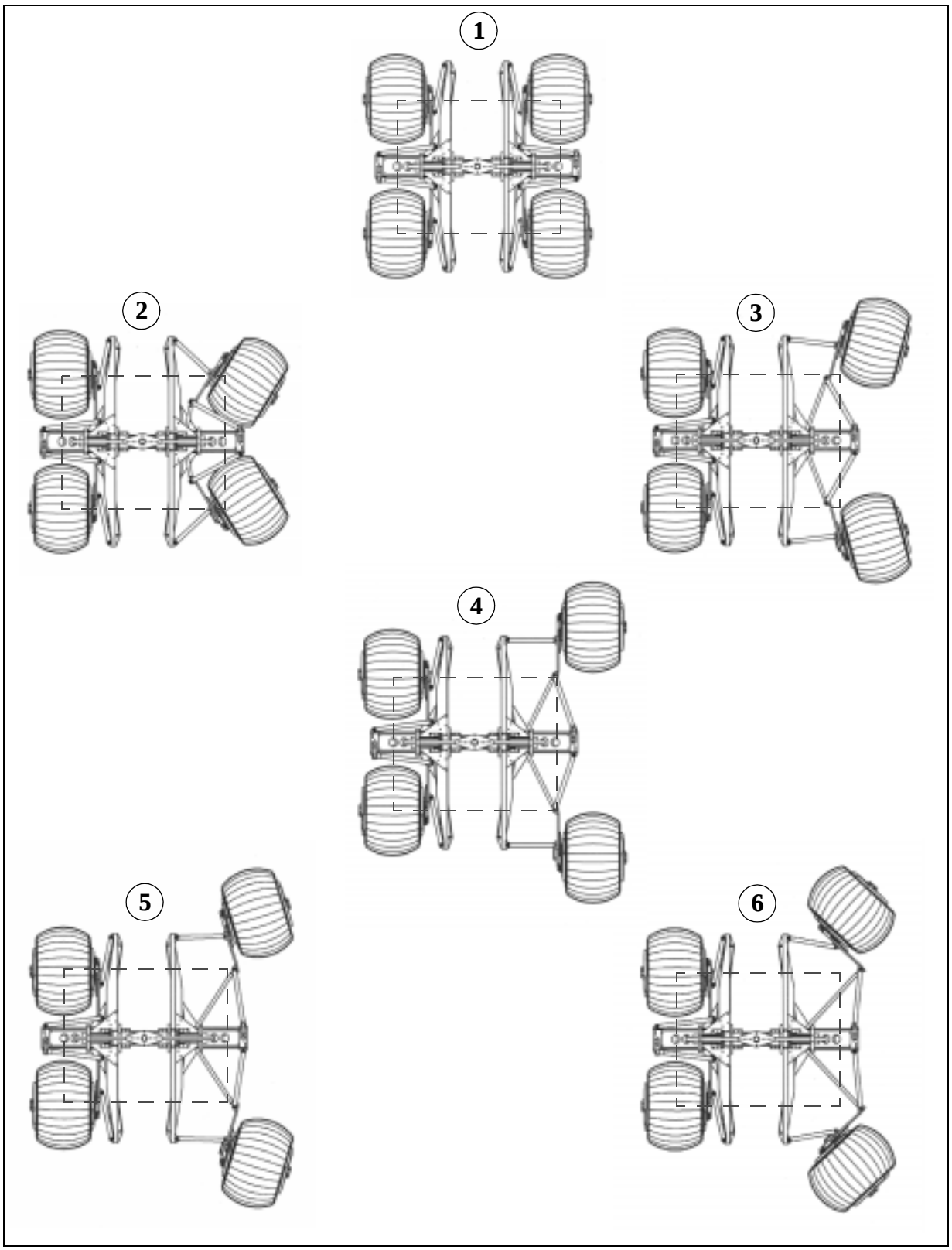

Figure 11: Nomad's Transforming Chassis

3.3 Internal Body Averaging

In order to distribute the normal forces on the wheels, Nomad has two floating side frames (called bogies). Each bogie is a structure that supports and deploys two wheels (left or right). By allowing the side frames to pivot on a central axle, the wheels can conform to uneven terrain and maintain even ground pressure. In order to stabilize the sensors mounted to the body, the two side frames are connected by means of a passive mechanical mechanism, enclosed in the chassis above the central axle. The averaging mechanism consists of a linkage attached to the middle of each of the side bogies. The central pivot of the averaging mechanism has a degree of freedom in the vertical direction, which is needed to allow the link to follow the bogies through a maximum wheel excursion of 50 cm. Body averaging of pitch and roll allows Nomad to have greater mobility while maintaining a high level of stability for accurate sensor readings.

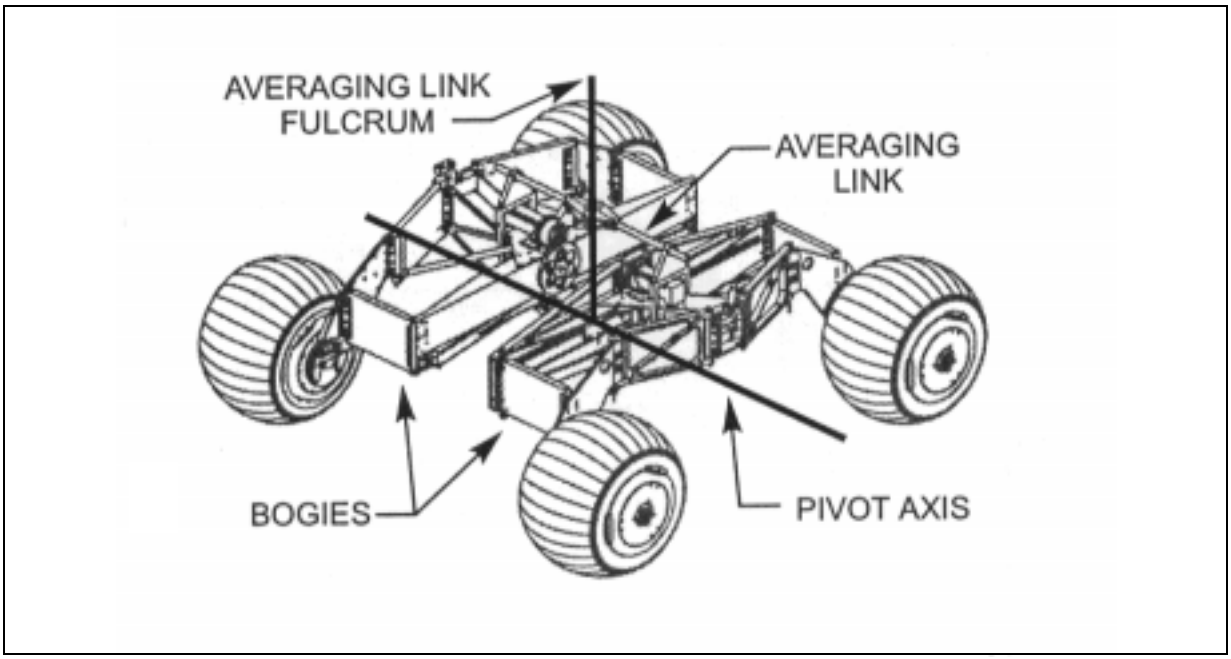

Figure 12: Averaging Mechanism

3.4 In Wheel Propulsion

Nomad features individual propulsion drive units that reside inside the wheel. This is unlike typical all-terrain vehicles, which have a central drive unit that distributes power to each of the wheels. The advantages of in-wheel propulsion include: sealed drive units, identical drive components, simplicity, and improved motion control.

The in-wheel propulsion unit is independent of the steering and suspension systems; no geometric or operational interferences occur between the systems. No electromechanical

components are needed for propulsion beyond those enclosed in the wheel (with the exception of the motor wires which are routed to the body fuselage through the deployment / steering linkages). This allows the drive components to be sealed within the wheel.

The motor and drivetrain assembly is at an offset distance below the wheel axle, which lowers the center of gravity of the wheel and simplifies its structural design and bearing selection. Triangular brackets suspend the drive assembly from the stationary axle. The motor is accessible for ease of removal and replacement if necessary. In the drive unit a brushless DC motor transmits torque and power to the wheel hub through a harmonic drive and a single stage gearing reduction. The output gear is mounted on the inside face of the outward facing wheel hub.

Simplicity (and thus reliability) is encouraged by eliminating mechanical transmission components and coupling assemblies. Only two bearings are needed to decouple the stationary wheel parts from the moving parts. Furthermore, the simplicity of the propulsion system imposes fewer constraints on the design of the chassis and the steering mechanism.

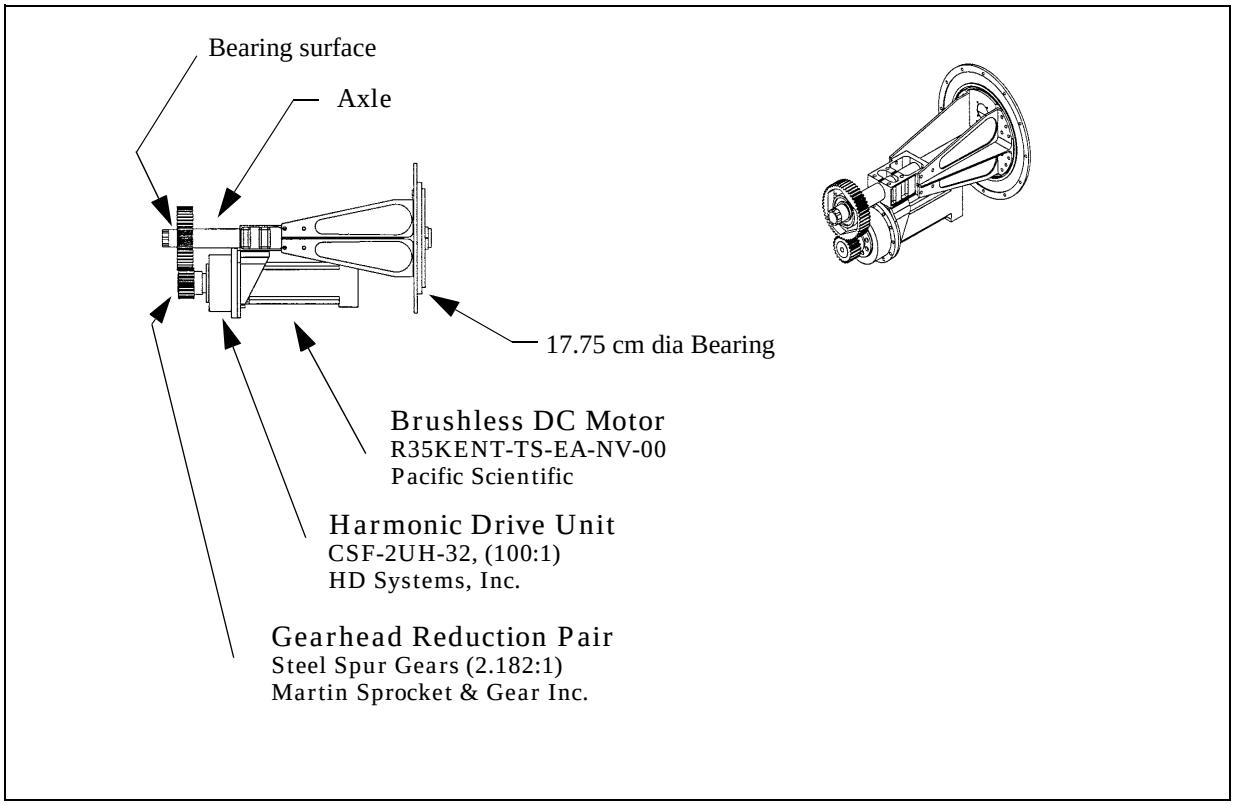

Figure 13: Wheel Module

Independent wheel actuation facilitates motion control and autonomous navigation. Wheel motion coordination is achieved electronically. Independent velocity-torque

control allows for closed-loop response to traction demands on each wheel.

3.5 Tire Design

The tire provides the surface area needed for traction and weight distribution. Typically the tire soil interaction provides the deformation that absorbs shock loading and diminishes suspension lift. Conventional tires succeed by using flexible elastomerics and pneumatic inflation to conform to terrain. However, in order to be space relevant the tires must be able to function effectively in an environment with a vacuum and temperature variations up to 100 degrees. The risk of deflation and decomposition of elastomers in such an environment prevents the use of the conventional approach.

Nomad relies on all-metal wheels to generate traction and negotiate terrain. The tire, which is the outmost portion of the wheel, is constructed of a thin aluminum shell manufactured to the shape of a wide-profile pneumatic tire. The compound curved shell provides maximum strength and resilience for minimum mass.

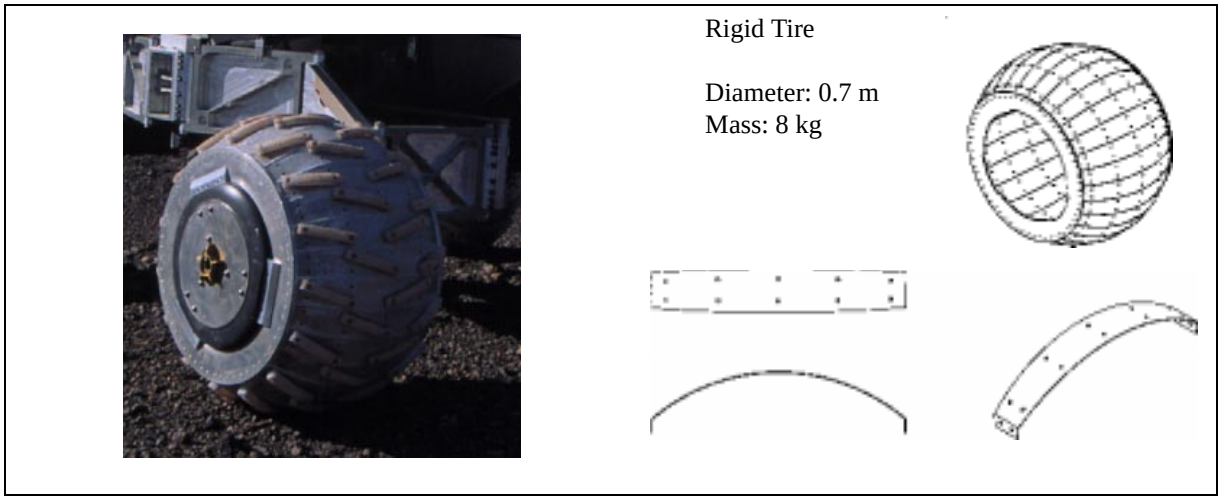

Figure 14: Tire Design

The rigid tire used on Nomad is composed of thirty strips of 6061-T6 Aluminum. The strips are cut and rolled so that when they are attached to the rims they form a solid shell. The strips are 2.3 mm thick and rolled to 0.711 m in diameter with a width of 0.43 m. The seams of the strips are welded to increase the strength of the shell. Such a wheel diameter reduces motion resistance due to soil compaction and sinkage, which in turn reduces bulldozing resistance. Despite the negative impact of a wider tire on steering resistance, the selected diameter to width ratio improves vehicle flotation and reduces ground contact pressure with positive effects on mobility in loose sand. The wheel behaves like a high-pressure pneumatic tire traversing frictional soil. The tire contact profile allows for

uniform load distribution over the contact patch and gradual soil compaction.

Grousers are attached to the tire to increase traction. A pattern similar to that used on tractors and other earth moving equipment is used. Each grouser is 7.6 cm long and 1.9 cm square. The shape and orientation of the cleats limits steering resistance on the tires as the chassis expands or contracts.

3.6 Performance

During June and July of 1997 Nomad traversed 223km in the Atacama Desert of southern Chile via transcontinental teleoperation. The primary objective of the Atacama Desert Trek was to develop, demonstrate, and evaluate a robot capable of long duration planetary exploration. The technology development focused on locomotion, imaging, communication, position estimation, safeguarded teleoperation, and remote science [Bapna98].

The highlights of the locomotion performance during the Atacama Desert Trek include traversing down slopes of 38 degrees and up slopes of 22 degrees. Discrete obstacles were surmounted up to 56 cm. The main contribution of the trek was to demonstrate capabilities for high performance planetary exploration by a mobile robot.

Chapter 4 Results

4.1 Results

Power and torque for skid and explicit turning degenerate to equal values at infinite radius (or straight driving). As the turn radius decreases from straight driving to a point turn, greater power and torque are required because a greater sideslip angle is encountered. For all turns skid steering requires greater power and torque than for explicit turning. This is because sideslip angles are greater in all cases. In the limiting case of a point turn, the power for skid steering is approximately double that for an explicit point turn. The primary contribution of this research is the experimental quantification of the power and torque requirements over turn radii from a radius equal to zero to an infinite radius.

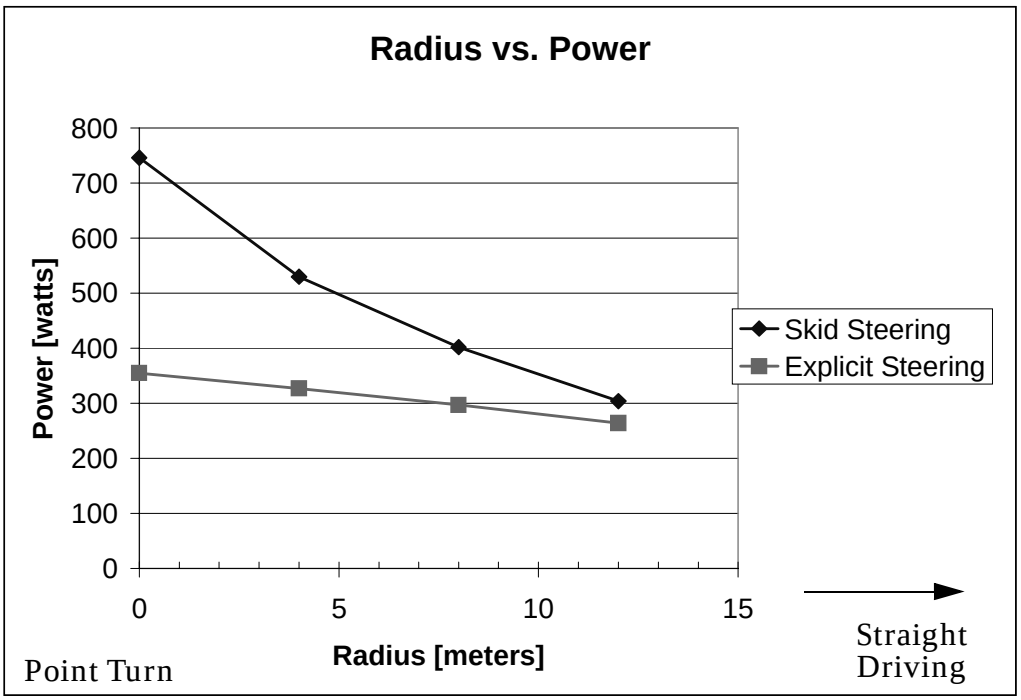

Figure 14: Experimental Results of Radius vs. Power for Nomad

4.2 Data Reduction

A digital filter is used in order to remove some of the noise from the velocity and current signals. The filter is of the form:

```
filt_data(n) = a * filt_data(n-1) + (1-a) * data(n)
```
[12]

The variable *data(n)* is the original data set of n points. The coefficient variable *a* is a smoothing factor.

The gps data is not filtered in any way. In order to analyze the gps data, the radius of each circle must be found. However, there are three unknowns: the x and y coordinates of the center of the circle, and the radius of the circle. By plotting the gps data it is easy to generate initial guesses for the unknown variables. A steepest descent numerical analysis is performed in order to determine the actual radius and the coordinates of the center of the circle. The evaluation function to be minimized is:

$$e = (x - \hat{x})^2 + (y - \hat{y})^2 - \hat{r}^2 \qquad [13]$$

The variables x, y, and $\hat{r}$ are the initial guesses for the x and y coordinates of the center of the circle and the radius of the circle. The variables x and y are the actual data points recorded during the experiments. The actual Matlab script used can be found in Appendix A.

4.3 Performance Parameters

4.3.1 Power

One key result is to compare the total power draw of the different steering maneuvers. Figure 15 shows the mean values of the power draw from the sum of each of the four driving motors during different steering maneuvers. The block of 150 watts is the mean no load power for the four wheels. No load power is obtained by running the four wheels at 15 cm/s while Nomad is raised off the ground. The power needed to drive the wheels while in the air shows the efficiency of the electrical and mechanical system. The fact that the no load power draw is such a significant portion of the driving power suggests that significant improvements can be made to the mechanical and electrical efficiency. The next block of varying power values shows the additional power required to perform the specified maneuver on gravel.

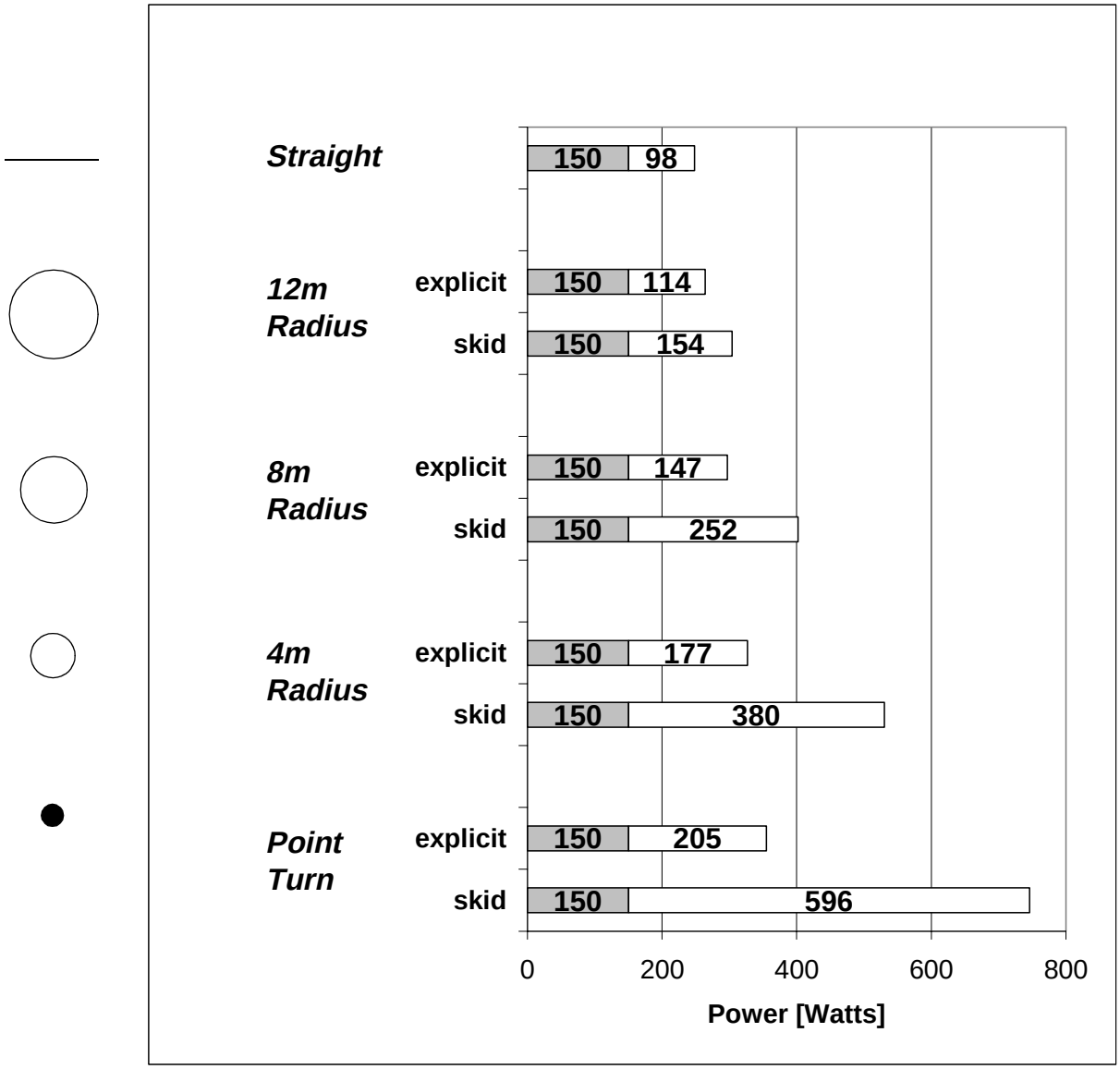

Figure 15: Power Draw vs. Radius

In order to provide non-dimensional values, the power of steady state steering is divided by the power to drive up a vertical wall, known as dead lift power.

$$Dead\ldots Lift\ldots Power = (mass)(velocity)(gravity) \quad [14]$$

$$(725kg)\left(0.15\frac{m}{s}\right)\left(9.8\frac{m}{s^2}\right) = 1065.8Watts \quad [15]$$

In order to provide a useful non-dimensional power value, only the power necessary to provide thrust on the terrain is used. No load power is removed since it varies significantly between different vehicles.

$$Non\text{–}dimensional\ldots Power = \frac{(Total\ldots Power) - (No\ldots Load\ldots Power)}{Dead\ldots Lift\ldots Power} \quad [16]$$

Figure 16 shows the plot of radius versus non-dimensional power. For the point turn, skid steering has a non-dimensional power value three times that of an explicit steer point turn. The non-dimensional power converges for both explicit and skid steering to a value of 0.1 at straight driving.

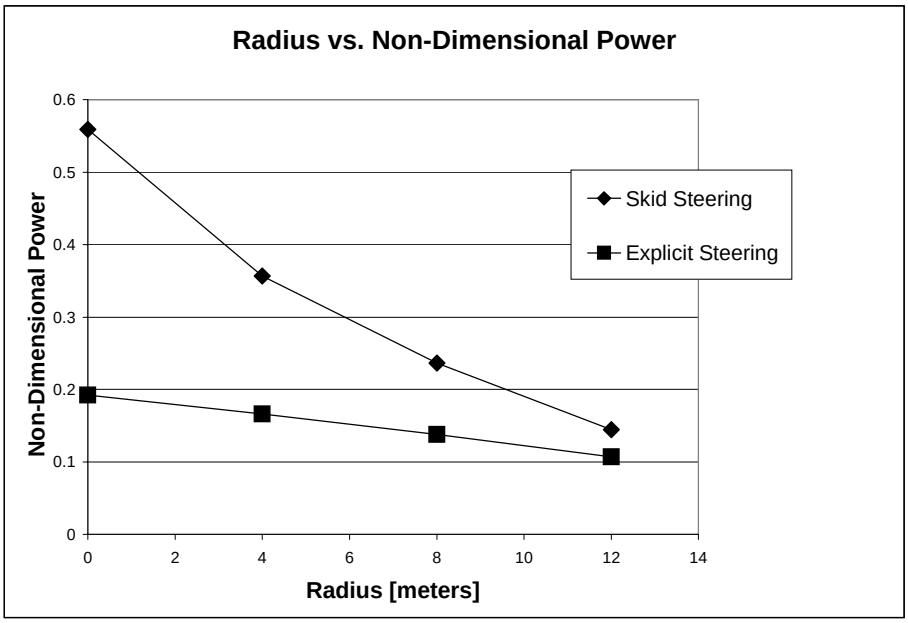

Figure 16: Radius vs. Non-Dimensional Power

4.3.1.1 Theoretical Power Draw

A theoretical prediction of power draw for a wheeled vehicle can be computed using relationships between vehicle and soil parameters developed by Bekker [Bekker69]. The theoretical power draw should be representative of the total power minus the no load power to remove the efficiencies of the mechanical and electrical components. Appendix B shows a sample calculation for Nomad driving at 15 cm/s using soil parameters of sand. Correct soil parameters were not gathered for the gravel terrain upon which Nomad performed the experiments. By changing a combination of soil values, a wide range of output power values can be obtained. This adds little value to the predicted power draw value unless the exact soil parameters are obtained. Therefore, the calculated value in the appendix is not representative of the power presented in the experimental results.

4.3.2 Position Data

Using differential gps the position of the center of the vehicle is recorded during steady state turning. Figure 17 shows a plot of vehicle position during skid steering for a desired radius of 4, 8, and 12 meters. The dotted line represents the desired radius in order to visualize the error (due primarily to a combination of longitudinal and side slippage).

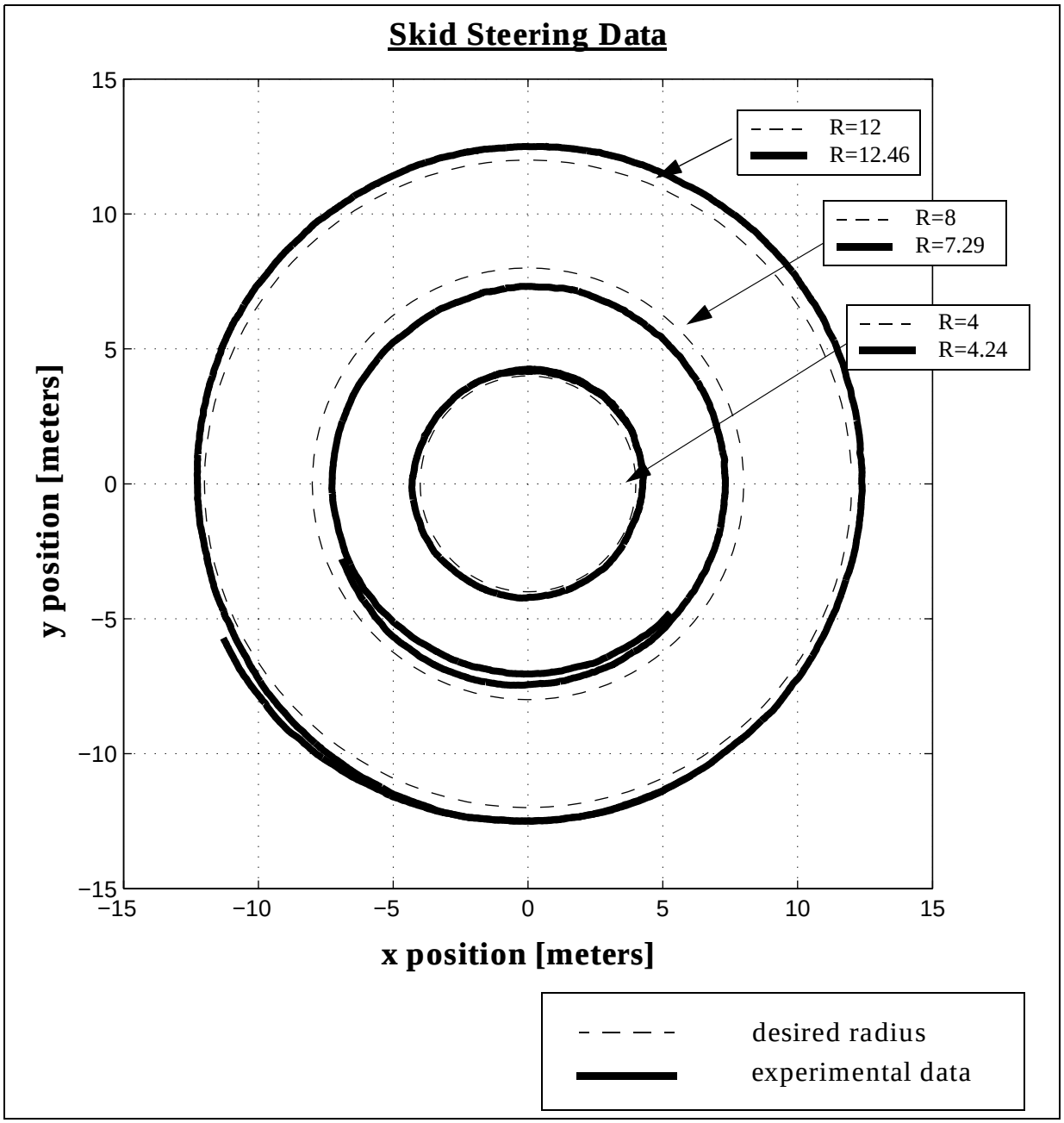

Figure 17: Experimental Skid Steer Position Data

Because no kinetic model exists for skid steering, only the kinematic model described in Chapter 1 is used to determine the outer and inner wheel velocities. On a trial and error basis the theoretical velocities from Table 1 were altered in order to reach the desired radii. The actual velocities used and the radii produced are shown in Table 3.

Table 3: Experimental Skid Steering Velocity Values

Actual Radius [m]	*Actual Vehicle Velocity V [m/s]*	*Inner Wheel Velocity v_i [m/s]*	*Outer Wheel Velocity v_o [m/s]*
4.2	**0.13**	**0.08**	**0.21**
7.3	**0.14**	**0.11**	**0.19**
12.5	**0.15**	**0.13**	**0.18**

The explicit steering results are not significantly better than skid steering except for the 8m radius turn. After modifying the inner and outer wheel velocities by 1 cm / s over three trials, the best result for skid steering is a radius of 7.3 meters.

For the purposes of this investigation geometric slip is defined as the ratio of the desired radius and the actual radius. The reason for the low slippage is that the slippage for driving straight has been removed by changing the wheel radius in the controller. The wheel radius used by the controller is 0.38 m; the actual wheel radius is 0.35 m with 1.9 cm grousers covering the surface of the wheel. The radius is changed experimentally in order to minimize slippage during normal operation.

Table 4: Geometric Slip

Radius [m]	**R_{actual} explicit**	**$R_{desired} / R_{actual}$ explicit**	**R_{actual} skid**	**$R_{desired} / R_{actual}$ skid**
4	**4.16**	**0.96**	**4.24**	**0.94**
8	**8.27**	**0.97**	**7.29**	**1.1**
12	**12.40**	**0.97**	**12.46**	**0.96**

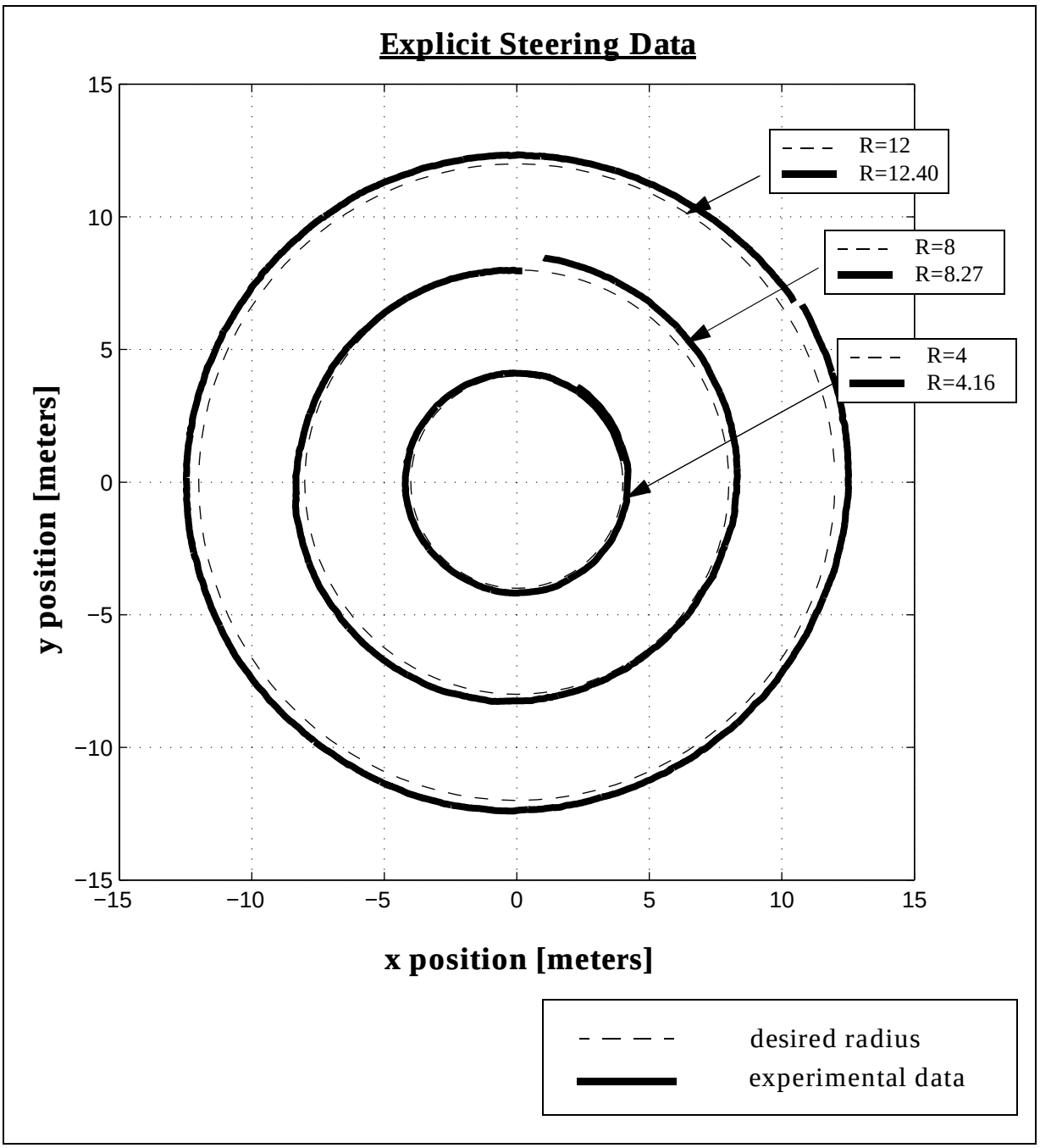

Figure 18: Experimental Explicit Steer Position Data

4.3.3 Wheel Torque

By monitoring the current of the drive motor amplifiers the torque used to propel each wheel can be estimated. The torque constant for the drive motors is given as 0.56 Nm / A. Using the gear reduction of 218, wheel torque can be determined. The torque values shown in the following figures are the total torque values, rather than torque values adjusted for the no load torque.

With the exception of the point turn, Figure 19 shows the wheel torques to be grouped within a 50 Nm band across the 4, 8, and 12 m turn radii. For straight driving the mean torque of the four wheels is 103 Nm. This matches the trend of the increased radius converging to straight driving.

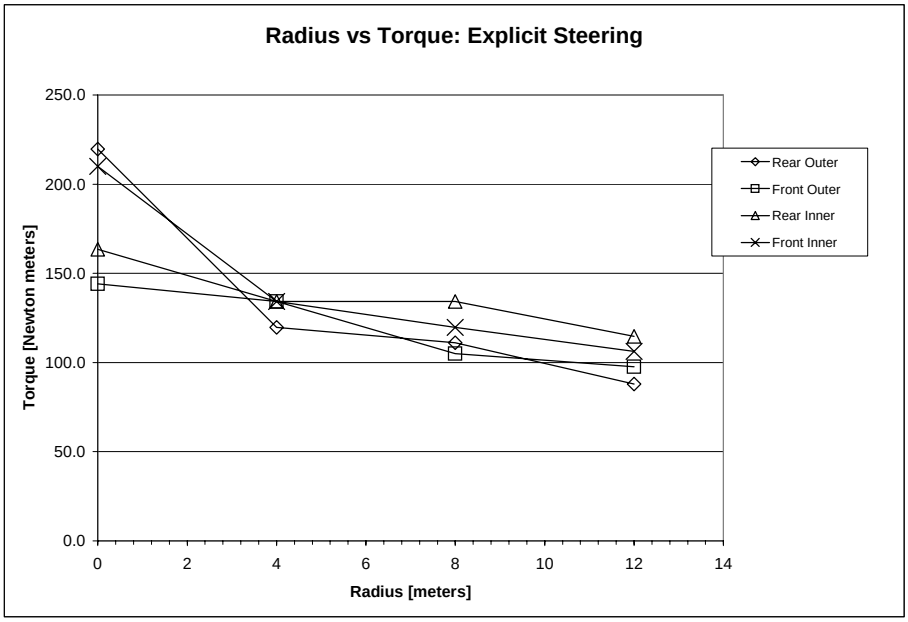

Figure 19: Radius vs. Torque: Explicit Steering

The explicit point turn shows a diagonal split in terms of torque values. The rear outer and front inner wheels carry most of the torque while the front outer and rear inner show significantly lower torque values.

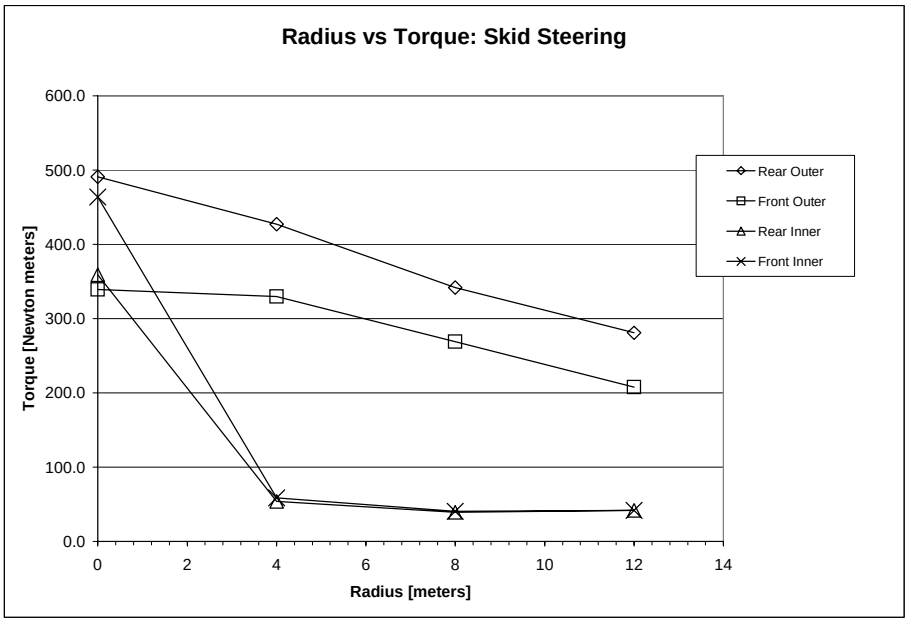

Figure 20: Radius versus Torque: Skid Steering

Figure 20 shows the torque values for skid steering. The skid steer point turn shows the same trend as the explicit point turn. Again, the torques are split in the same diagonal fashion with the rear outer and front inner carrying 150 Nm more than the front outer and rear inner wheels. As the radius increases the rear outer wheel consistently carries between 75 and 100 Nm more than the front outer wheel. In order to determine if the rear outer wheel consistently carries more torque than the other wheels, the direction of turn was modified for the 4m radius skid steer turn. A counterclockwise and a reverse clockwise turn were performed, as shown in Figure 21. The results in Figure 21 show that, independent of turn direction, the rear outer wheel has a consistently higher torque value than the other wheels.

.

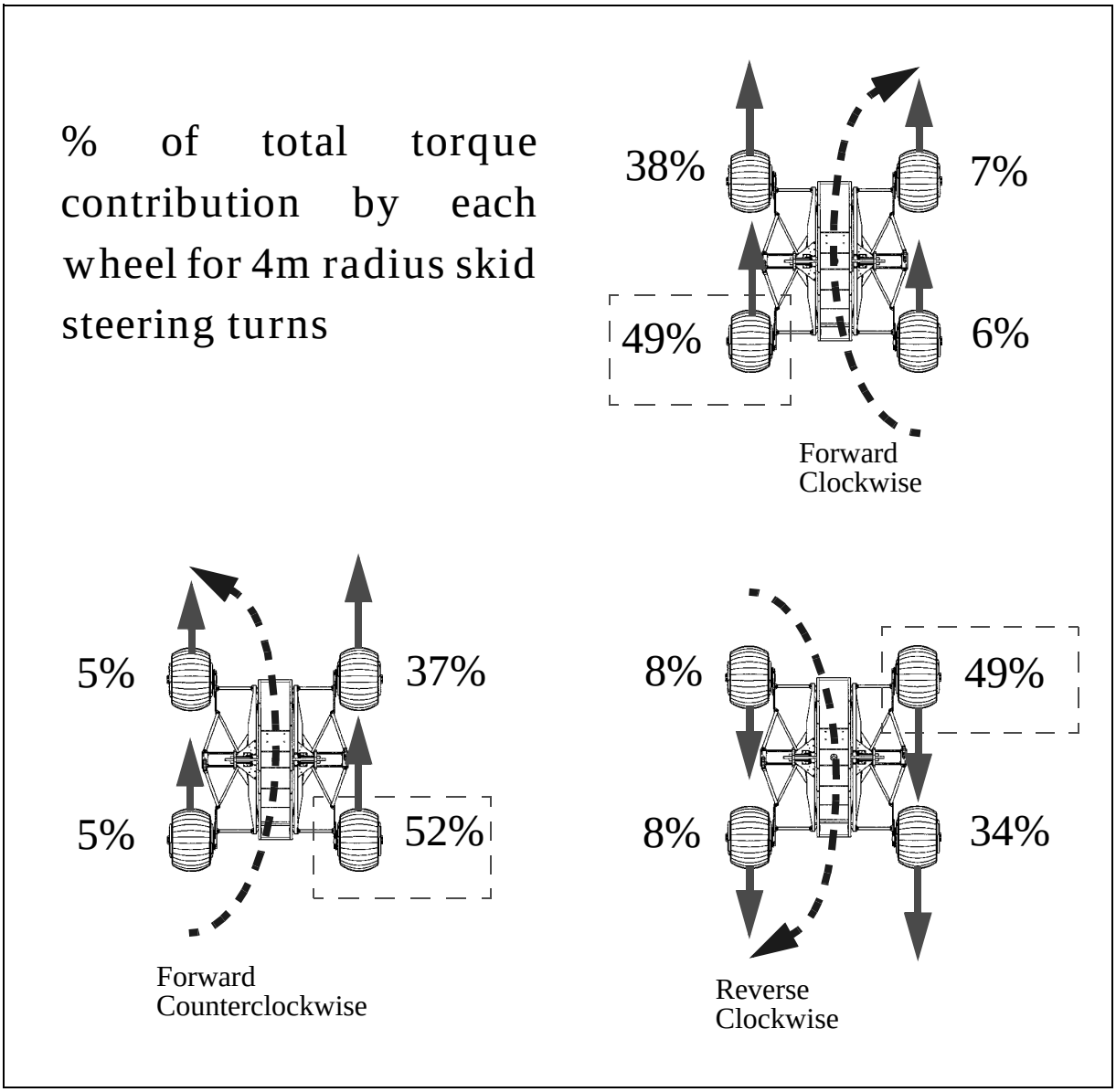

Figure 21: Individual Wheel Torque: Skid Steering

One observation that can be made about the higher torque in the rear outer wheel is that the phenomenon occurs only when the lateral force is pushing from the outside of the wheel. This observation is consistent with the torque values of the point turn, in which the wheels with lateral forces stemming from outside the wheel require higher torque. The lateral resistance pushing from the outside of the wheel could be affecting the forces on the gears (which are located on the outside of the wheel). The drive gears are cantilevered from the inner wheel linkage. If the lateral forces on the outside of the wheel are producing a deflection of the gear support structure, increased torque would be

needed to turn the wheel. However, further investigation is needed to prove if such deflection is occurring.

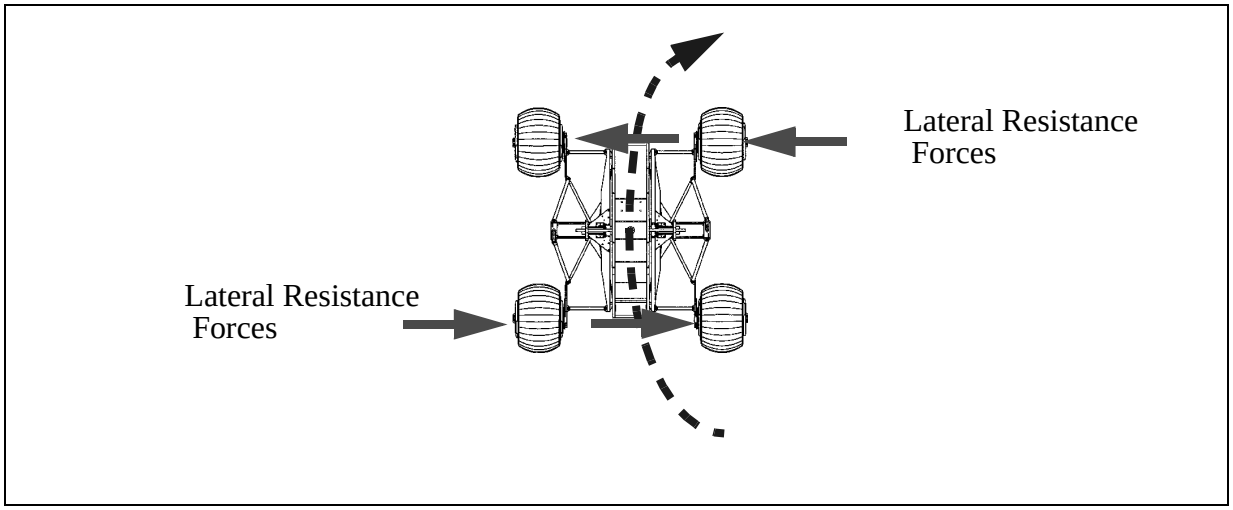

Figure 22: Lateral Forces While Skid Steering

4.4 Path Energy

The energy required to traverse a given path can be computed using the results of the power required for steady state turning over a range of turning radii. Given a path a comparison can be made of the energy consumption between skid steering and explicit steering.

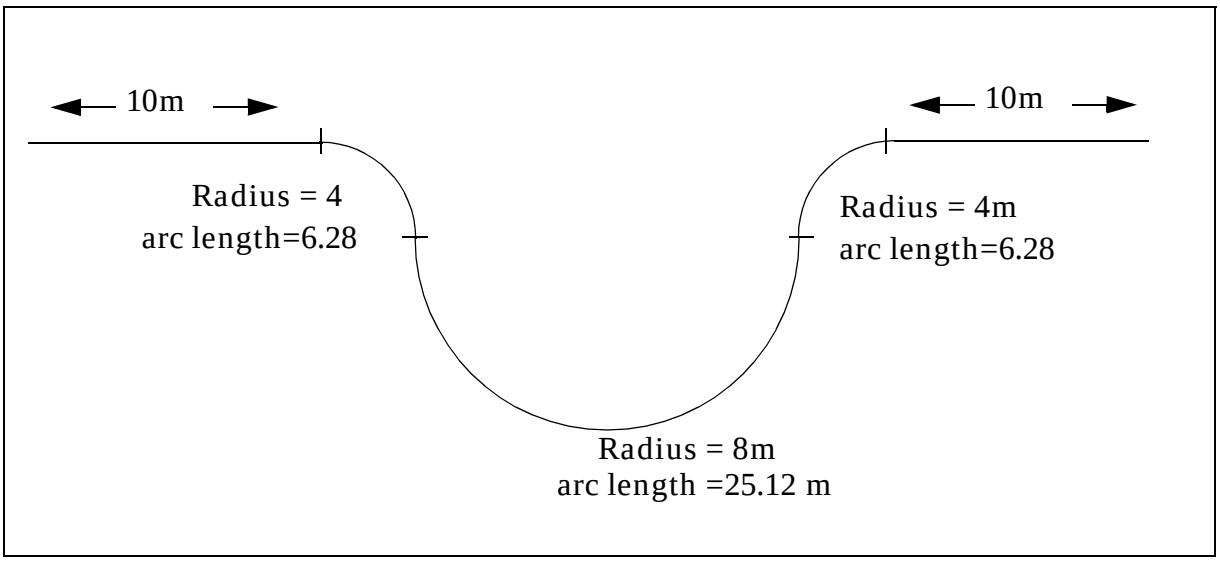

Figure 23: Example Path

The path energy is computed by taking the path distance divided by the vehicle velocity multiplied by the power required for that driving maneuver. For example, for the 4 m

radius portion the energy required for explicit and skid steering is:

$$energy_{explicit(R=4)} = \frac{6.28m}{0.15\frac{m}{s}}\left(327\frac{Nm}{s}\right) = 13.7kJ \quad [17]$$

$$energy_{skid(R=4)} = \frac{6.28m}{0.15\frac{m}{s}}\left(530\frac{Nm}{s}\right) = 22.2kJ \quad [18]$$

The total energy to traverse the path shown in Figure 23 is 96.7 kJ for explicit steering and 122.8 kJ for skid steering. This simple example shows how the results of the quantification of explicit and skid steering maneuvers can be used to determine the energy required to traverse a specific path.

4.5 Error

These results may be complicated by several factors. First, statistical significance was not achieved. All tests were performed only once; as a consequence it is possible that these results may not be repeatable. Additionally, the testing was performed over a period of several months. As a result, the terrain may have changed over time. For example, changes in moisture content and temperature could influence the resistance of the soil, and thus the torque required to drive on the terrain.

The use of no load power to remove the inefficiencies of the mechanical and electrical components assumes that the inefficiencies do not change over the loaded condition. When Nomad is driving on terrain, bearing and gear losses might differ due to differences in loading factors. The performance of the generator and electrical components may also vary during load intensive tests.

Torque values are generated by using the constant of 0.56Nm / A, a constant provided by the motor manufacturer. The assumption that the torque per amp is constant does not hold when the motor draws a peak current for high loading conditions. Thus, the torque constant could vary under high loading conditions. A more precise measure of torque would be to use a torque sensor mounted directly on the motor shaft.

Another source of error is the wheel alignment. Each tire contains a number of welds, each of which might induce error in tire shape and alignment. Inconsistencies in tire shape or alignment induce error into the velocity measurements for each individual wheel.

Chapter 5 Conclusion

5.1 Accomplishments

The primary accomplishment of this research is the quantification of power draw values for a range of radii for both explicit and skid steering of a wheeled rover. This work has relevance to the optimization of rover designs in light of steering performance requirements. Mobile robot power sources always have the potential to limit performance. By quantifying the amount of power used for both explicit and skid steering, educated decisions can be made about the most appropriate steering configuration for a specific application.

5.2 Perspectives

This thesis argues that explicit steering draws significantly less power than skid steering during tight turning maneuvers. However, for large radius turns the power draw during skid steering converges to the values observed during explicit steering.

Based on this research, a simpler two wheel steer vehicle would be able to successfully complete the same 200km traverse performed by Nomad without significant changes in power draw. The tight turning capabilities of Nomad were not necessary during general driving of the Atacama Desert Trek. In retrospect, I would have focused on a softer suspension to alleviate the shock vibrations encountered during the traverse rather than the intricate steering mechanism. However, part of the complexity of Nomad's steering mechanism stems from the ability to stow the wheels in order to create a compact vehicle for transport. The stowing capability did allow Nomad to be transported in a 747 airplane without disassembly; this would not have been possible if Nomad remained in the deployed position. For planetary missions, where volume and weight have such high costs, vehicle storage for transport is critical.

The locomotion assembly of Nomad contains approximately 450 different components (not including fasteners or wiring). Each of the four drive units contains 32 components

leaving 315 parts that are involved with the support and actuation of the steering mechanism. I suspect that a skid steer vehicle such as RATLER [Klarer 94] contains less than 200 parts for the entire locomotion assembly. Such a low part count has positive implications on reliability and mass.

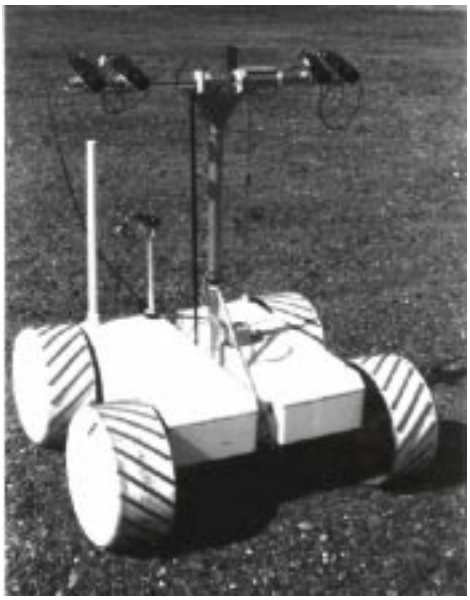

Figure 24: Robotic All Terrain Exploration Rover

5.3 Future Work

5.3.1 Development of the Kinetic Steering Model

The most significant weakness of this research is the lack of an analytical model that could be used to predict the power and torque required for explicit and skid steering maneuvers. The kinematic equations do not take into account the slippage between the wheels and the soil. The slippage requires an increase in power and torque over the values predicted by the kinematic equations of turning. A general model of turning would use vehicle parameters, soil parameters, turn radius, and wheel velocities as inputs. The output variables would be wheel torque, power, and side slip angle.

5.3.2 Slope turning

The claim that skid steering while driving up a slope will be refused before explicit steering has not been confirmed by this research. While a skid steering vehicle has the advantage of a low part count and mass, aggressive turning can be limited. Such aggressive turning maneuvers such as steering while driving up a slope have yet to be quantified experimentally.

5.3.3 Varying Test Parameters

The experiments presented show specific results for steady state turning. Within the experiments variables such as the distribution of wheel loading, vehicle velocity, and soil parameters should be varied to provide a more complete analysis of steady state turning.

5.3.4 Current Control

Changing the drive wheel control strategy from velocity control to current control is one way to study the efficiency of torque control. Holding the velocity constant forces the wheels to slip as they pass over paths of different lengths which is inefficient. For example, when one wheel passes over an obstacle it must travel further than the other wheels traveling on flat ground.

5.4 Closure

This research examines power and torque requirements for the steady state turning of a wheeled rover. Although this work is limited in scope because it only studies flat ground and offers a limited number of test results, differences between skid and explicit steering are still apparent. As wheeled rovers become more prevalent, similar tests can be performed on different platforms. As this happens it will be possible to expand on this initial work so as to describe the performance of different vehicles over a variety of maneuvers and terrain types.

References

[Apostolopoulos98] Apostolopoulos, D., "Analytical Configuration of Wheeled Robotic Locomotion," P.h.D. Thesis, Carnegie Mellon University, Robotics Institute, May 1998.

[Bapna97] Bapna, Deepak et. al., "Atacama Desert Trek: A Planetary Analog Field Experiment," Proceedings of i-SAIRAS'97, Tokyo, Japan, July 14-16, 1997, pp. 355-360.

[Bapna98] Bapna, Deepak et. al., "The Atacama Desert Trek: Outcomes," Proceedings of ICRA 98, Leuven, Belgium, May 1998, pp 597-604.

[Bekker60] Bekker, M., G., "Mobility of Cross Country Vehicles -Thrust for Propulsion-, Floatation and Motion Resistance-, -Track and Wheel Evaluation-, -Optimum Performance and Future Trend-", Series of articles in: Machine Design, Penton Publishing Co., Cleveland Ohio, December 24, 1959; January 7, 1960; January 21, 1960; February 4, 1960.

[Bekker64] Bekker, M., G., "Mechanics of Locomotion and Lunar Surface Vehicle Concepts", Transactions of the Society of Automotive Engineers, Vol. 72, 1964, pp. 549-569.

[Bekker69] Bekker, M., G., Introduction to Terrain-Vehicle Systems, University of Michigan Press, Ann Arbor, MI, 1969.

[Bickler92] Bickler, D. B., "A New Family of Planetary Vehicles," International Symposium on Missions, Technologies, and Design of Planetary Mobile Vehicles, Toulouse, France, 1992.

[Boeing92] The Boeing Company, Advanced Civil Space Systems Division. "Piloted Rover Technology Task 9.4 Final Report," NASA Contract NAS8-37857, 1992.

[Costes72] Costes, N., C., et al., "Mobility Performance of the Lunar Roving Vehicle: Terrestrial Studies - Apollo 15 Results," NASA TR R-401, 4th International

Conference of the International Society for Terrain-Vehicle Systems, Stockholm and Kiruna, Sweden, April 24-28, 1972.

[Dudzinski89] Dudzinski, Piotr, A., "Design Characteristics of Steering Systems for Mobile Wheeled Earthmoving Equipment", Journal of Terramechanics, Vol. 26, No. 1, pp. 25-82, 1989.

[Hayati96] Hayati, S., et al., "Microrover Research for Exploration of Mars," Proceedings of the AIAA Forum on Advanced Developments in Space Robotics, University of Wisconsin, Madison, August 1-2, 1996.

[Itoh90] Itoh, H., and Oida, A., "Dynamic Analysis of Turning Performance of 4WD-4WS Tractor on Paved Road," Journal of Terramechanics, Vol. 27, No. 2, pp. 125-143, 1990.

[Itoh94] Itoh et al., "Meaurement of Forces Acting on 4WD-4WS Tractor Tires During Steady -State Circular Turning on a Paved Road," Journal of Terramechanics, Vol. 31, No. 5, pp. 285-312, 1994.

[Itoh95] Itoh et al., "Meaurement of Forces Acting on 4WD-4WS Tractor Tires During Steady -State Circular Turning in a Rice Field," Journal of Terramechanics, Vol. 32, No. 5, pp. 263-283, 1995.

[Klarer94] Klarer, P., "Recent Developments in the Robotic All Terrain Lunar Exploration Tover Program," ASCE Specialty Conference on Robotics for Challenging Environment, Albuquerque, NM, 1994.

[nytimes98] The New York Times on the web, http://www.nytimes.com/library/national/science/072198sci-mars.html, July 21, 1998.

[Wong93] Wong, J., Y., Theory of Ground Vehicles, John Wiley & Sons, Inc., New York, NY, 1993.

Appendix A GPS Data Modeling

A.1

The following is the matlab script used to model the gps data:

```
function par = circle2(xdata, ydata, xhat, yhat, rhat, TOL);
% function par = circle2(xdata, ydata, xhat, yhat, rhat, TOL);
%
% Finds the value of xhat, yhat, rhat to minimize the minimum mean
% squared error in the model (x-xhat)^2 + (y-yhat)^2 - rhat^2
% for the data given in xdata and ydata.  TOL tells how closely
% the parameters are optimized.

[m,c] = size(xdata);
[n,d] = size(ydata);
if (m~=n)
  disp 'xdata and ydata are not the same size'
  return;
end
if ((c~=1)|(d~=1))
  disp 'xdata and ydata are not single column vectors'
  return;
end

alpha = 0.1;

delta = TOL+1;

while (delta > TOL)
   e = ((xdata-xhat ).*(xdata-xhat) + (ydata-yhat).*(ydata-yhat) - rhat*rhat);
   E = e' * e;
   dEdxhat = -4/(n^2) * e' * (xdata-xhat);
   dEdyhat = -4/(n^2) * e' * (ydata-yhat);
   dEdrhat = sum( -4 * e' * rhat )/(n^2);
   xhat = xhat - alpha * dEdxhat;
   yhat = yhat - alpha * dEdyhat;
   rhat = rhat - alpha * dEdrhat;
   delta = sqrt(dEdxhat.^2 + dEdyhat.^2 + dEdrhat.^2);
   par = [xhat yhat rhat];
end

par = [xhat yhat rhat]';
```

Appendix B Kinetics

B.1 Straight Driving Kinetics

Straight driving serves as a baseline for comparison with steady state turning. A force diagram shows that the force needed to turn a wheel is equal and opposite to the resistance provided by the soil.

The thrust needed to provide vehicle locomotion is derived from the interaction between the wheel and the soil. The soil provides the resistance needed for locomotion until the soil shears. This shearing ultimately produces a slip condition in which the wheel spins without providing any vehicle thrust.

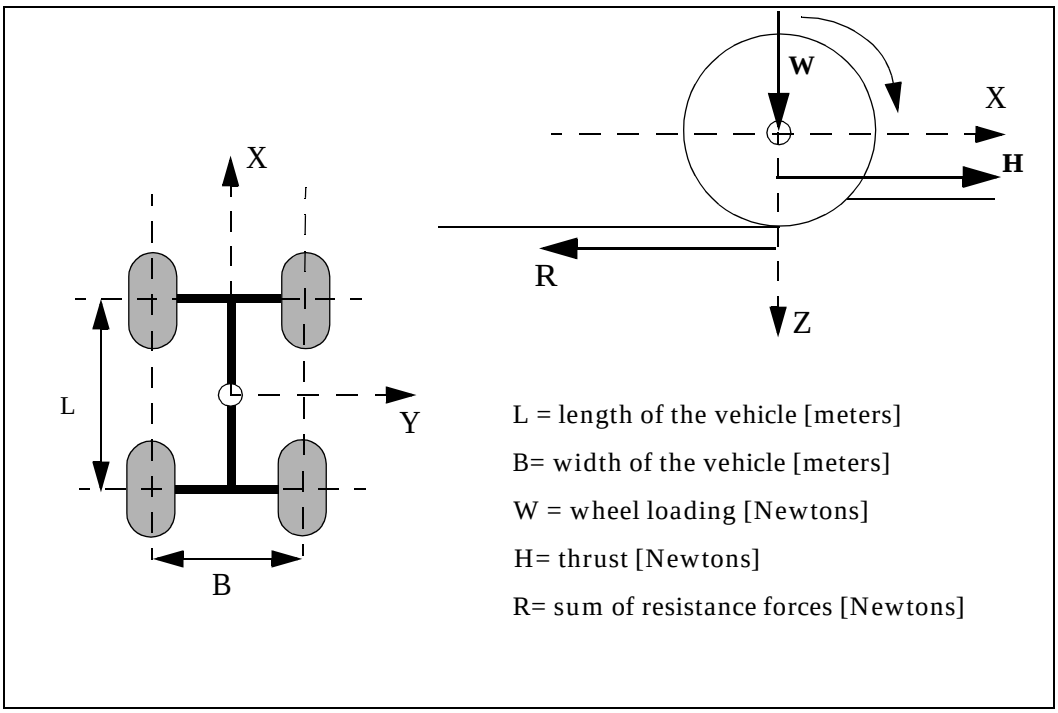

Figure 25: Force Diagram for Straight Driving

The determination of resistance forces is dependent on a physico-geometrical relationship between terrain and the vehicle [Bekker64]. The relationship has been

determined with the use of vehicle and soil parameters. The soil parameters can be determined using a standardized set of tests.

Table 5: Vehicle Parameters

Input	*Symbol*	*Units*
vehicle length	l	meters
vehicle width	b	meters
wheel loading	W_w	Newtons
wheel diameter	d_w	meters
wheel width	b_w	meters
vehicle velocity	v	meters/sec

Table 6: Soil Parameters

Input	*Symbol*	*Units*
exponent of sinkage	n	
cohesive modulus of soil deformation	k_c	N/m^{n+1}
frictional modulus of soil deformation	k_ϕ	N/m^{n+2}
cohesion of soil	c	Pascals
angle of internal friction	ϕ	degrees
coefficient of rolling friction	f_r	

All of the following equations can be referenced from [Apostolopolous98].

The sinkage of a rigid wheel on flat ground is calculated from the following:

$$z = \left(\frac{3W_w}{(3-n)(k_c + b_w k_\phi)(\sqrt{d_w})} \right)^{\frac{2}{(2n+1)}} \quad [19]$$

The motion resistance is divided into compacting, bulldozing, and rolling resistance. Compacting resistance is found from:

$$R_c = \frac{\left(\frac{3W_w}{\sqrt{d_w}} \right)^{\frac{2n+2}{2n+1}}}{\left(\left((3-n)^{\frac{2n+2}{2n+1}} \right)(n+1)(k_c + b_w k_\phi)^{\frac{1}{2n+1}} \right)} \quad [20]$$

Bulldozing resistance is found from:

$$R_b = \left(0.5\alpha b_w z^2\left(\tan\left(45+\frac{\phi}{2}\right)\right)^2\right) + 2cb_w z\left(\tan\left(45+\frac{\phi}{2}\right)\right) \quad [21]$$

Rolling resistance is:

$$R_r = f_r W_w \quad [22]$$

Therefore the total resistance for a single wheel is computed from the sum of all the resistance forces:

$$R_{tot} = R_c + R_b + R_r \quad [23]$$

The drive torque for a single wheel can then be computed from the resistance force:

$$T_w = (R_{tot})\left(\frac{d_w}{2}\right) \quad [24]$$

The power draw needed to provide the necessary torque is:

$$P_w = T\left(\frac{2v}{d_w}\right) \quad [25]$$

From this analysis, given soil parameters, vehicle dimensions, and mass, theoretical values for torque and power can be calculated. The soils parameters are given for the example of Nomad driving on sand. Data is unavailable for the experiments performed on gravel as presented in the Chapter 4.

Table 7: Input Values for Theoretical Analysis of Straight Driving

Input	*Symbol*	*Value*	*Units*
vehicle length	L	1.83	meters
vehicle width	B	1.97	meters
wheel loading	W_w	1780	Newtons
wheel diameter	d_w	0.711	meters
wheel width	b_w	0.457	meters
vehicle velocity	V	0.15	meters/sec
exponent of sinkage	n	1.1	
cohesive modulus of soil deformation	k_c	0.689	kN/m^{n+1}
frictional modulus of soil deformation	k_ϕ	1058.6	kN/m^{n+2}

Input	*Symbol*	*Value*	*Units*
cohesion of soil	c	1.04	kPa
angle of internal friction	ϕ	28.0	degrees
coefficient of rolling friction	f_r	0.05	

Table 8: Theoretical Results for Straight Driving of a Single Wheel

Output	*Symbol*	*Value*	*Units*
sinkage	z	3.54	centimeters
compaction resistance	R_c	298	Newtons
bulldozing resistance	R_b	72.84	Newtons
rolling resistance	R_r	88.96	Newtons
drive torque	T	163.6	Newton meters
drive power	P	69	Watts

The total drive power of 276 watts is calculated by multiplying the value for a single wheel (69 watts) by four. This value serves as an example of the theoretical power needed for Nomad to drive on sandy terrain at 15 cm/s.

Appendix C Sensing and Control

C.1 Schematic

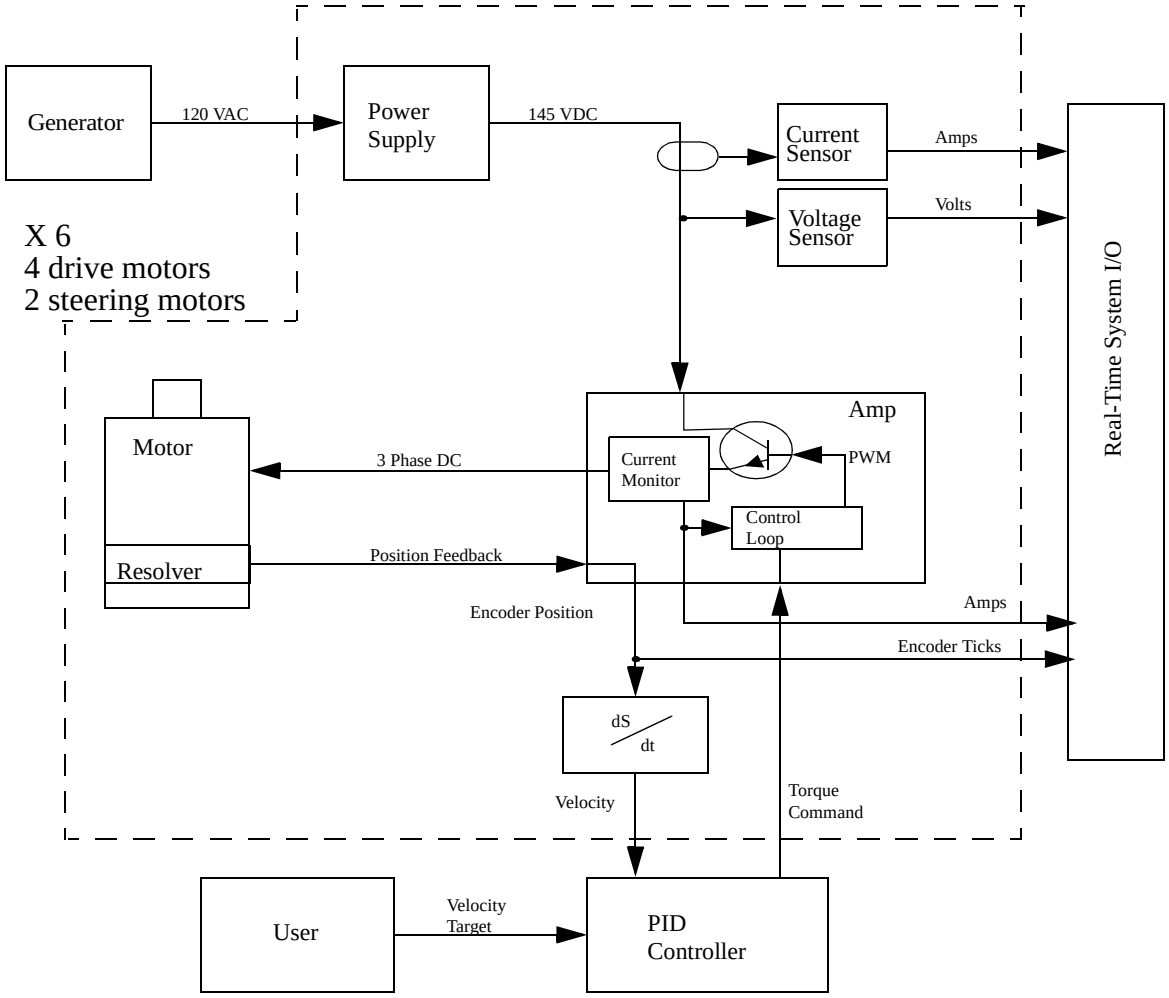

Figure 26: Sensing and Control Diagram

Appendix D Steering Activity

D.1 Metric Postulation

In order to compare the mobility and use of a given steering configuration a new metric is formulated. As a preliminary formulation, without rigorous derivation, the metric of steering activity takes into account the distance travelled by the inner and outer wheels divided by the distance traveled by the vehicle center.

$$SA = \left[\int_0^S \left(\frac{|owp| - |iwp|}{|vcp|} \right) \right] \quad [26]$$

where:

S = the total path length

vcp = the vehicle center path length

owp = the outer wheel path length

iwp = the inner wheel path length

A singularity occurs when the path length of the outer and inner wheels is nonzero but the path length of the vehicle center is zero. This causes the expression to have a zero term in the denominator. Such a singularity occurs when the vehicle performs a point turn.

Given the path shown in Figure 27 the steering activity can be computed. For straight line driving the steering activity is zero because the outer wheel path length and the inner wheel path length are equivalent. For a vehicle of width two the steering activity for the four meter radius turn (traversing 1/4 of a circle) is computed as follows (where B is the vehicle width):

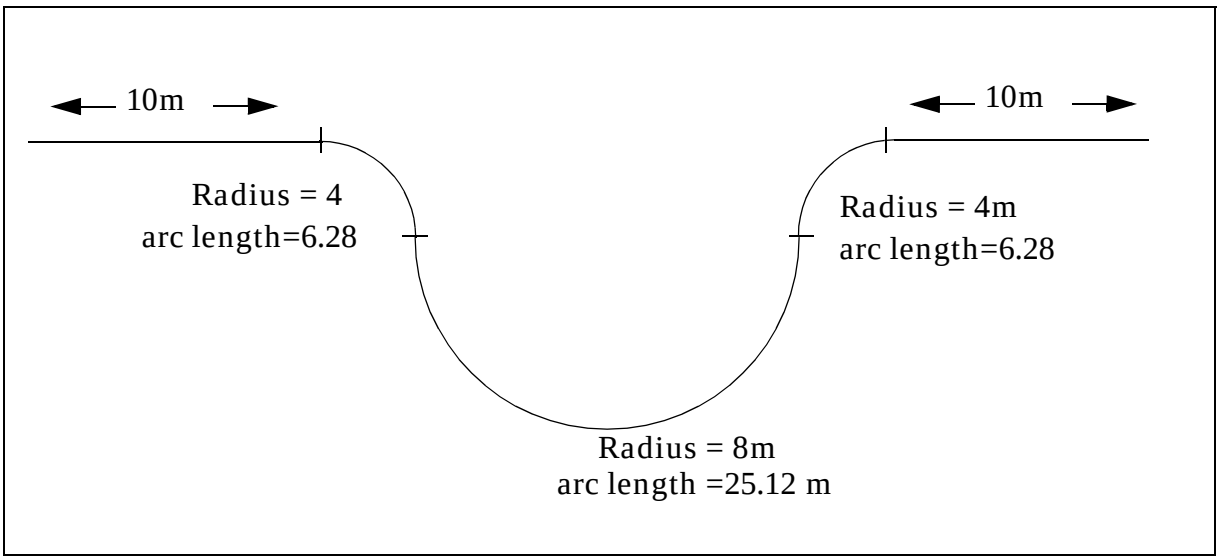

Figure 27: Example path

$$vcp = \frac{2\pi r}{4} = \frac{2\pi 4}{4} = 2\pi \quad [27]$$

$$owp = \frac{2\pi\left(r + \frac{B}{2}\right)}{4} = \frac{2\pi\left(4 + \frac{2}{2}\right)}{4} = \frac{5}{2}\pi \quad [28]$$

$$iwp = \frac{2\pi\left(r - \frac{B}{2}\right)}{4} = \frac{2\pi\left(4 - \frac{2}{2}\right)}{4} = \frac{3}{2}\pi \quad [29]$$

Therefore, the steering activity for a four meter turn with a heading change of 90 degrees is:

$$SA_{R=4} = \frac{\frac{5}{2}\pi - \frac{3}{2}\pi}{2\pi} = \frac{1}{2} \quad [30]$$

The steering activity for the eight meter radius is computed in a similar fashion. Therefore the steering activity of the entire path shown in Figure 27 is found.

$$SA = SA_{R=4} + SA_{R=8} + SA_{R=4} = \frac{1}{2} + \frac{1}{4} + \frac{1}{2} = 1.25 \quad [31]$$